The CD4 transmembrane GGXXG and juxtamembrane (C/F)CV+C motifs mediate pMHCII-specific signaling independently of CD4-LCK interactions

Mark S. Lee[1], Peter J. Tuohy[1], Caleb Y. Kim[1], Philip Yost[1], Katrina Lichauco[1], Heather L. Parrish[1], Koenraad Van Doorslaer[1, 2, 3, 4, 5, 6], and Michael S. Kuhns[1, 3, 4, 5, 6]

[1] Department of Immunobiology, The University of Arizona College of Medicine, Tucson, AZ 85724, USA.

[2] School of Animal and Comparative Biomedical Sciences, The University of Arizona, Tucson, AZ 85724, USA.

[3] Cancer Biology Graduate Interdisciplinary Program and Genetics Graduate Interdisciplinary Program, The University of Arizona, Tucson, AZ 85724, USA.

[4] The BIO-5 Institute, The University of Arizona, Tucson, AZ 85724, USA.

[5] The University of Arizona Cancer Center, Tucson, AZ, USA

[6] The Arizona Center on Aging, The University of Arizona College of Medicine, Tucson, AZ, USA

[*]Correspondence: vandoorslaer@arizona.edu, mkuhns@email.arizona.edu

Running title: The CD4 GGXXG and (C/F)CV+C motifs are key determinants of pMHCII-specific signaling.

Abstract

$CD4^+$ T cell activation is driven by 5-module receptor complexes. The T cell receptor (TCR) is the receptor module that binds composite surfaces of peptide antigens embedded within MHCII molecules (pMHCII). It associates with three signaling modules (CD3γε, CD3δε, and CD3ζζ) to form TCR-CD3 complexes. CD4 is the coreceptor module. It reciprocally associates with TCR-CD3-pMHCII assemblies on the outside of a $CD4^+$ T cells and with the Src kinase, LCK, on the inside. Previously, we reported that the CD4 transmembrane GGXXG and cytoplasmic juxtamembrane (C/F)CV+C motifs found in eutherian (placental mammal) CD4 have constituent residues that evolved under purifying selection (Lee, et al., 2022). Expressing mutants of these motifs together in T cell hybridomas increased CD4-LCK association but reduced CD3ζ, ZAP70, and PLCγ1 phosphorylation levels, as well as IL-2 production, in response to agonist pMHCII. Because these mutants preferentially localized CD4-LCK pairs to non-raft membrane fractions, one explanation for our results was that they impaired proximal signaling by sequestering LCK away from TCR-CD3. An alternative hypothesis is that the mutations directly impacted signaling because the motifs normally play an LCK-independent role in signaling. The goal of this study was to discriminate between these possibilities. Using T cell hybridomas, our results indicate that: intracellular CD4-LCK interactions are not necessary for pMHCII-specific signal initiation; the GGXXG and (C/F)CV+C motifs are key determinants of CD4-mediated pMHCII-specific signal amplification; the GGXXG and (C/F)CV+C motifs exert their functions independently of direct CD4-LCK association. These data provide a mechanistic explanation for why residues within these motifs are under purifying selection in jawed vertebrates. The results are also important to consider for biomimetic engineering of synthetic receptors.

57 **Introduction**

58 Delineating the mechanistic principles by which multi-module receptors drive complex
59 biological processes is important both for our broad understanding of receptor biology,
60 and for guiding biomimetic engineering of synthetic receptors for therapeutic purposes.
61 For example, the design of conventional single-chain chimeric antigen receptors (CARs)
62 utilized in CAR-T cell therapy was informed by an early 1990's understanding of
63 receptor biology and bears little resemblance to the multi-module receptors that
64 naturally drive T cell responses. These design differences necessitate that conventional
65 CARs integrate with the T cell intracellular signaling machinery differently than their
66 natural counterparts, leading us to posit that fully coopting T cell functions with synthetic
67 receptors requires that they be designed to integrate with the T cell's intracellular
68 signaling machinery in a way that mimics the native receptors (Harris and Kranz, 2016;
69 Kobayashi et al., 2020; Wu et al., 2020). Achieving this goal requires a more complete
70 understanding of the multi-module receptors that mediate antigen-specific T cell
71 activation. In particular, understanding how $CD4^+$ T cells respond to antigen is important
72 for informing biomimetic engineering of CARs because recent data show that redirecting
73 $CD4^+$ T cells with CARs is important for long-lived therapeutic efficacy (Melenhorst et
74 al., 2022).

75 $CD4^+$ T cells are driven by 5-module receptors that recognize peptide antigens
76 embedded within MHCII (pMHCII). Each naïve $CD4^+$ T cell expresses a clonotypic
77 receptor module, called the T cell receptor (TCR), that binds specifically to unique
78 features of composite pMHCII surfaces (Kuhns and Badgandi, 2012; Kuhns and Davis,
79 2012). The TCR lacks intracellular signaling domains and instead assembles with three

80 signaling modules (CD3γε, δε, and ζζ) that have immunoreceptor tyrosine-based
81 activation motifs (ITAMs), and other motifs, to connect TCR-pMHCII interactions to the
82 intracellular signaling apparatus. CD4 is the coreceptor module. It binds pMHCII in a
83 reciprocal fashion with TCR-CD3 on the outside of $CD4^+$ T cells and interacts with the
84 Src kinase, LCK, via an intracellular CQC zinc clasp motif and helix (Huse et al., 1998;
85 Kim et al., 2003). According to the TCR signaling paradigm, co-engagement of pMHCII
86 by TCR-CD3 and CD4 positions LCK and the CD3 ITAMs in the proper spatial proximity
87 to enable LCK phosphorylation of the CD3 ITAMs to initiate signaling (Rudd, 2021).
88 However, when we tested this model directly we found that CD4-LCK interactions are
89 not key determinants of CD3ζ ITAM phosphorylation (pCD3ζ)(Lee et al., 2022). Based
90 on our work and that of other labs, including a study showing that C-terminally truncated
91 CD4 lacking the motifs that mediate CD4-LCK interactions can nevertheless drive $CD4^+$
92 T cell development, proliferation, and T-helper functions, we consider the question of
93 how intracellular pMHCII-specific $CD4^+$ T cell signaling is initiated to be unresolved
94 (Glassman et al., 2018; Horkova et al., 2023; Killeen and Littman, 1993; Xu and Littman,
95 1993).
96 The answer to this question lies with how the 5 modules of pMHCII receptors
97 evolved over ~435 million years to refine pMHCII-specific signaling. We have therefore
98 taken a systems biology approach to computationally analyze data from real world
99 experiments performed in 99 jawed vertebrate species under a variety of conditions
100 over the course of evolution. By computationally reconstructing the evolutionary history
101 of CD4, we identify residues and motifs in the extracellular, transmembrane, and
102 intracellular domains that are of predicted to be functionally important (Lee et al., 2022).

103 We then cross-validated these findings using a well-established T cell hybridoma
104 experimental system (58$\alpha^-\beta^-$ cells) wherein we performed structure-function analysis of
105 mutants of key motifs to infer their function by evaluating the phenotypes of the mutants
106 relative to the wildtype (WT). When we mutated the intracellular CQC clasp and IKRLL
107 helix motifs that are known to mediate CD4-LCK interactions, we observed significant
108 reductions in CD4-LCK association; yet we did not observe the predicted decrease in
109 CD3ζ ITAM phosphorylation (pCD3ζ). In contrast, when we mutated the
110 transmembrane GGXXG motif and cytoplasmic juxtamembrane (C/F)CV+C
111 palmitoylation motif, we observed an increased frequency of CD4-LCK pairs that were
112 preferentially localized to detergent soluble membrane domains. We also found
113 evidence of reduced CD3ζ, ZAP70, and PLCγ1 phosphorylation (pCD3ζ, pZAP70, and
114 pPLCγ1) compared with WT CD4. The reason that constituent residues of these motifs
115 evolved under purifying selection therefore appears to be due to reduced signaling in
116 response to pMHCII when the motifs are altered. We took these data as evidence that
117 the GGXXG and (C/F)CV+C motifs arose in eutherians (placental mammals) to tightly
118 regulate pMHCII-specific signal initiation and postulated that the mutant CD4 molecules
119 might sequester LCK away from TCR-CD3 to prevent CD3ζ phosphorylation. An
120 alternative hypothesis is that the GGXXG and (C/F)CV+C motifs impact pCD3ζ levels
121 independently of CD4-LCK interactions.
122 In the present study we tested these hypotheses by studying the impact of
123 GGXXG and (C/F)CV+C motif mutants individually, or together, on proximal pMHCII-
124 specific signaling in C-terminally truncated CD4 molecules (T1). Working with T1
125 eliminated motifs in the intracellular domain, including those that mediate CD4-LCK

126 association. As expected from prior work, truncating CD4 relieved CD4-LCK interactions
127 and reduced IL-2 production. However, there was no impact on the average pCD3ζ
128 levels or the percent of cells with phosphorylated CD3ζ when compared with WT CD4,
129 despite significantly reduced levels of CD4-LCK pairs. These data provide further
130 evidence that the core tenet of the TCR signaling paradigm, wherein CD4 recruits LCK
131 to CD3 ITAMs initiates signaling, needs revising. Importantly, T1 molecules bearing
132 mutations in the GGXXG and (C/F)CV+C motifs individually or together reduced IL-2
133 production as well as pCD3ζ levels and other TCR-proximal signaling events. The
134 simplest interpretation of these data is that the GGXXG and (C/F)CV+C motifs are key
135 determinants of pMHCII-specific signaling on their own, independent of CD4-LCK
136 interactions.
137
138 **Results**
139 The goal of this study was to evaluate if the transmembrane GGXXG and
140 juxtamembrane (C/F)CV+C palmitoylation motifs, which are highly conserved in
141 eutherians (placental mammals) and contain constituent residues under purifying
142 selection (**Figure 1**), influence pMHCII-specific proximal signaling on their own rather
143 than by sequestering CD4-LCK pairs away from membrane rafts. Accordingly, we used
144 58$\alpha^-\beta^-$ T cell hybridomas transduced to express the 5c.c7 TCR along with either the WT
145 or mutant CD4 constructs described in **Table 1**. The well-characterized 5c.c7 TCR
146 recognizes the moth cytochrome c peptide 88-103 (MCC) in the context of mouse
147 MHCII I-E^k. We used this experimental system because 58$\alpha^-\beta^-$ cells were used in
148 seminal work to link CD4-LCK association to IL-2 production (Glaichenhaus et al.,

149 1991). Specifically, mutating or removing the intracellular CQC clasp motif was shown in
150 that study to reduce both CD4-LCK association and signaling output as measured by IL-
151 2 production. We confirmed those findings in our recent study (Lee et al., 2022).
152
153 **WT and T1 equivalently enhance pMHCII-specific proximal signaling.** Previously
154 we reported that the C-terminally truncated mouse CD4 T1 mutant (**Table 1 and Figure**
155 **1 arrow**) reduces but does not prevent IL-2 production relative to WT CD4 despite
156 lacking most of the intracellular domain, including the CQC clasp and IKRLL motifs
157 shown to mediate CD4-LCK association (Lee et al., 2022). Because T1 maintains both
158 the transmembrane GGXXG and juxtamembrane (C/F)CV+C motifs, we reasoned that it
159 had utility for studying the contributions these motifs make to pMHCII-specific signaling
160 in the absence of CD4-LCK interactions.
161 Accordingly, we generated 5c.c7^{+} 58$\alpha^{-}\beta^{-}$ cells expressing WT CD4, T1, or T1
162 combined with our previously reported Δbind mutant that disrupts binding to pMHCII in
163 the CD4 D1 domain. This T1$^{\Delta bind}$ mutant allowed us to eliminate the contributions of
164 CD4-pMHCII interactions as well as CD4-LCK interactions (**Table 1 and Figure 2 –**
165 **figure supplement 1**)(Glassman et al., 2016; Glassman et al., 2018; Parrish et al.,
166 2015). The goals were to: 1) determine if T1 significantly impairs pMHCII-specific
167 signaling events, relative to WT, as expected because it lacks the CQC and IKRLL
168 motifs that mediate CD4-LCK interactions; 2) use T1$^{\Delta bind}$ to establish the baseline above
169 which pMHCII-dependent assembly of CD4 with TCR-CD3 contributes to signaling. The
170 T1 mutant produced measurable IL-2 (response magnitude ~61% of WT, **Table 2**) that
171 was consistently reduced across a range of MCC peptide concentrations compared to

172 WT, whereas the T1$^{\Delta bind}$ mutant did not produce IL-2. We also observed reduced
173 pMHCII-specific endocytosis for T1 and T1$^{\Delta bind}$ compared to WT (**Figure 2A and Figure**
174 **2 – figure supplement 2**). These data indicate that, in our system, extracellular CD4-
175 pMHCII engagement is essential for IL-2 production while the CD4 intracellular domain
176 C-terminal of R422 contributes to IL-2 production, but is not absolutely necessary in the
177 absence of other elements of the intracellular domain.

178 Next, we evaluated the impact of these mutations on proximal signaling events
179 measured by flow cytometry in response to antigen presenting cells (APCs) expressing
180 agonist MCC:I-E^k after background subtraction of signal levels in response to APCs
181 expressing null Hb:I-E^k (**Figure 2 – figure supplement 3**). Our analysis of five
182 independently generated pairs of WT and T1 cell lines showed variable difference in
183 pCD3ζ levels. For three pairs of lines, the T1 response was higher than the WT and for
184 two it was lower (**Figure 2B**). The averages of the T1 response normalized to the paired
185 WT controls showed no difference between the population. There were also no
186 differences for the average percent of T1 cells with response levels to MCC that were
187 above background responses to the null Hb peptide compared to their paired WT
188 controls. Similar results were observed for pZAP70 and pPLCγ1 levels (**Figure 2 –**
189 **figure supplement 4**). These data, summarized in **Table 2,** provide evidence that CD4-
190 LCK interactions via the CQC clasp and IKRLL motifs are not key determinants of
191 pMHCII-specific early signal events in this experimental system.

192 In comparison, the T1$^{\Delta bind}$ mutant significantly reduced pCD3ζ, pZAP70, or
193 pPLCγ1 levels compared to the T1 control but, interestingly, did not impact the percent
194 of cells responding to agonist MCC:I-E^k (**Figure 2C and Figure 2 – figure supplement**

195 **5**). Because the antibodies used to detect pCD3ζ, pZAP70, and pPLCγ1 recognize
196 single phosphorylated tyrosines, these data indicate that CD4 enhances the number of
197 TCR-CD3 complexes per cell with phosphorylated CD3ζ molecules at Y142 (same in
198 human and mouse), as well as the number of phosphorylated ZAP70 and PLCγ1
199 molecules per cell, in a manner that is dependent on TCR-CD3 and CD4 co-
200 engagement of pMHCII but independent of the intracellular domain C-terminal of R422.
201 A summary of these results can be found in **Table 3**. A key takeaway is that the
202 average pCD3ζ levels for three independently generated $T1^{\Delta bind}$ mutants was 54.86% of
203 the T1 control ($p<0.001$). CD3ζ phosphorylation therefore occurs upon TCR
204 engagement of cognate pMHCII in the absence of CD4-pMHCII interactions, and CD4
205 engagement of pMHCII increases the number of phosphorylated TCR-CD3 complexes.
206 Importantly, the pCD3ζ levels observed in the $T1^{\Delta bind}$ mutants is subthreshold for IL-2
207 production at the bulk population level. These results allow us to conclude that pMHCII-
208 specific baseline pCD3ζ levels achieved in our system in the absence of CD4-pMHCII
209 interactions are approximate half of that achieved when CD4 can interact with pMHCII
210 on the outside of the cell. Furthermore, consistent with the kinetic discrimination model
211 of T cell activation, CD4-pMHCII interactions on the outside of the cell appear to be
212 essential to push pCD3ζ levels above the threshold level needed for IL-2 production
213 (Rabinowitz et al., 1996).
214

215 **The GGXXG and (C/F)CV+C motifs influence IL-2 production independently of**
216 **LCK.**

217 Having established that T1 contributes to early pMHCII-specific signaling (e.g. pCD3ζ)

218 as well as signaling output (i.e. IL-2), we generated 5c.c7^{+} 58$\alpha^{-}\beta^{-}$ cells expressing WT,
219 T1, or T1 bearing mutants of the GGXXG and/or (C/F)CV+C motifs (**Table 1 and Figure**
220 **3 – figure supplement 1**). To study the function of the GGXXG motif alone, we used
221 our previously described TMD mutant (GGXXG to GVXXL) wherein bulky side chains
222 replace the glycines that compose a flat surface on the transmembrane helix that could
223 mediate protein:protein or protein:cholesterol interactions (Fessler, 2016; Parrish et al.,
224 2015; Song et al., 2014; Teese and Langosch, 2015; Wacker et al., 2013). We called
225 these mutants T1-TMD. To test the function of the palmitoylation motif, which contains
226 the core CVRC (418-421) sequence in mouse and humans, we made note of a broader
227 (C/F)CVRC motif in eutherians wherein the majority of ortholog sequences had CCVRC,
228 as found in mouse, and a minority had FCVRC as found in humans. Importantly,
229 position 417 is under purifying selection for all extant CD4 orthologs we analyzed by the
230 fixed effects likelihood (FEL) method (**Figure 1**), indicating that this residue evolved
231 under purifying selection due to functional importance (Lee et al., 2022). We therefore
232 made T1-Palm (3C) mutants wherein we mutated all three cysteines to serines as well
233 as T1-Palm (2C) mutants where only the core cysteines common to mouse and humans
234 were mutated to serines. Finally, we made mutants containing both the TMD and Palm
235 mutants that we called T1-TP(3C) or T1-TP(2C).
236 To confirm that truncating CD4 relieved CD4-LCK association, and evaluate if the
237 mutations impacted any residual CD4-LCK interactions that may occur due to
238 colocalization in particular membrane domains, we performed sucrose gradient analysis
239 of detergent lysates of WT, T1, T1-TMD, T1-Palm(2C), T1-Palm(3C), T1-TP(2C) and
240 T1-TP(3C). We observed significantly reduced CD4-LCK association in detergent

241 resistant membranes (DRMs, aka membrane rafts) and detergent soluble membranes
242 (DSMs) for T1 compared to WT (**Figure 3 – figure supplement 2**)(Pike, 2006). The
243 mutants did not impact residual CD4-LCK association in the DRMs or DSMs.
244 Furthermore, the total LCK signal associated with CD4 was significantly lower for T1
245 compared with the WT, and the residual association was not impacted by the mutants
246 (**Table 3 and Figure 3 – figure supplement 3**). We therefore conclude that, in our
247 experimental system, any functional differences between the T1-TMD, T1-Palm(2C/3C),
248 or T1-TP(2C/3C) mutants and the T1 control is a function of the motif we are studying in
249 the absence of direct CD4-LCK interactions.
250 Next, we measured IL-2 production by WT, T1, and CD4 mutant cells to evaluate
251 the impact of the mutations on signaling output in response to MCC. Here again, T1
252 was slightly lower than WT, while the T1-TMD reduced the IL-2 response magnitude
253 and sensitivity relative to the T1 control (**Figure 3A**). This was expected given our prior
254 work showing that the TMD mutant reduced IL-2 production driven by a shorter CD4
255 truncation mutant (CD4T, mutated at R420)(Parrish et al., 2015). Mutating the GGXXG
256 or (C/F)CV+C motifs individually or together did not impact pMHCII-induced TCR
257 endocytosis relative to the T1 control, and activation-induced CD4 endocytosis was
258 inhibited for all truncated CD4 molecules (**Figure 3 – figure supplement 4A and 4B**).
259 The T1-Palm(2C), T1-TP(2C), T1-Palm(3C), and T1-TP(3C) all reduced IL-2 production
260 relative to T1, indicating that they also influence the LCK-independent contribution of
261 CD4 to pMHCII-specific signaling (**Figure 3B**). Of note, the T1-TP(2C) IL-2 response
262 magnitude was lower than that of T1-Palm(2C) alone, consistent with what we
263 previously observed with the full-length versions of these CD4 mutants (**Figure 3B**)(Lee

264 et al., 2022). Furthermore, the T1-Palm(3C) response magnitude was lower than that of
265 T1-Palm(2C), suggesting that the additional cysteine contributes to signaling. Together,
266 these data indicate that the GGXXG and (C/F)CV+C motifs contribute to the signaling
267 cascade that leads to pMHCII-specific IL-2 production when CD4 does not directly
268 interact with LCK via the intracellular CQC clasp and IKRLL motifs. These data do not
269 tell us where in the signaling pathway the contributions are made.
270
271 **The CD4 GGXXG and (C/F)CV+C motifs are key determinants of early signaling.**
272 To evaluate if the GGXXG and (C/F)CV+C motifs influence early signaling events, we
273 measured pCD3ζ, pZAP70, and pPLCγ1 levels for four independently generated T1-
274 TMD lines, three independently generated T1-Palm(2C) lines, and three independently
275 generated T1-TP(2C) lines relative to their matched T1 controls in response to APCs
276 expressing MCC:I-E^k (**Figure 4 and Figure 4 – Figure supplement 1 and 2, and**
277 **Table 3**). For the T1-TMD, T1-Palm(2C), and T1-TP(2C) mutant lines we observed
278 lower average levels of pCD3ζ, pZAP70, and pPLCγ1 relative to the T1 controls. These
279 data indicate that the GGXXG and (C/F)CV+C motifs contribute to CD4's ability to
280 enhance proximal signaling in the absence of CD4-LCK interactions.
281 Of note, when we considered the average fold change of the means of the
282 independently generated mutant cell lines relative to their paired T1 controls, we
283 included the mean of the fold change of the $T1^{\Delta bind}$ mutant cells from Figure 2C relative
284 to their paired T1 controls for comparison (**dotted line, Figure 4B and Figure 4 –**
285 **Figure supplement 1B and 2B**). Doing so provides visual boundaries within which to
286 consider the contribution that CD4 T1, which can bind pMHCII, makes to proximal

287 signaling in relationship to T1$^{\Delta bind}$ (dotted line) that cannot bind pMHCII. These
288 boundaries then provide an additional guide for evaluating the impact of the mutations
289 on proximal signaling. For example, the T1-TMD and T1-Palm(2C) showed reduced
290 pCD3ζ levels midway between T1 and T1$^{\Delta bind}$, which equated to a reduced contribution
291 to pCD3ζ levels made by these mutants to ~48% of the contribution to pCD3ζ levels
292 made by T1, while the T1-TP(2C) contributed ~16% of the pCD3ζ levels contributed by
293 T1. The double mutant therefore nearly eliminated the contribution made by T1 to
294 pCD3ζ levels. Although these are relative comparisons, the data further suggest a role
295 for the GGXXG and (C/F)CV+C motifs in contributing to CD4-mediated pMHCII-specific
296 signaling in the absence of CD4-LCK interactions.
297 Because we had found that T1$^{\Delta bind}$ cells failed to produce IL-2 in response to high
298 peptide concentrations in our dose response experiments (**Figure 1A**), whereas the T1-
299 TP(2C) mutant cells made IL-2 in response to high peptide concentrations (**Figure 3B**),
300 we found it interesting that the early signaling responses we measured to APCs
301 expressing high ligand densities of tethered pMHCII were similar between the T1$^{\Delta bind}$
302 and T1-TP(2C) cells. We therefore evaluated IL-2 production of the T1, T1$^{\Delta bind}$, and T1-
303 TP(2C) in response to the APCs used in these signaling studies to ask if they followed
304 the same pattern of responses to high peptide doses in our prior experiments. We found
305 that the T1-TP(2C) cells made approximately half as much IL-2 as the T1 controls,
306 whereas IL-2 production by the T1$^{\Delta bind}$ cells was negligible (**Figure 4 – Figure**
307 **supplement 3**). These data indicate that the ability of CD4 to interact with pMHCII can
308 partially overcome the loss of function of the GGXXG and (C/F)CV+C motifs at high
309 ligand densities with respect to a downstream signaling output, such as IL-2 production,

310 even if the early signaling events measured at 2 minutes after pMHCII-engagement
311 were similar.
312 Finally, we considered the percent of responders (i.e., those cells that signaled
313 above background) for the mutant cell lines. We observed small decreases in
314 responding T1-TP(2C) cells for pCD3ζ and pZAP70 relative to the control, while pPLCγ1
315 trended lower for this mutant. These data indicate that mutating the GGXXG and
316 (C/F)CV+C motifs together in the absence of the intracellular domain can reduce the
317 number of cells that initiate pMHCII-specific signaling (**Figure 4C and Figure 4 –**
318 **Figure supplement 1C and 2C**). We did not observe this phenotype in our prior study
319 when the intracellular domain was present, suggesting this is unique to the absence of
320 the intracellular domain (Lee et al., 2022).
321 We also measured early signaling for three independently generated T1-
322 Palm(3C) and T1-TP(3C) mutant cell lines compared to their paired T1 controls. For all
323 lines, pCD3ζ, pZAP70, and pPLCγ1 levels were significantly lower than the controls,
324 which was reflected in the normalized fold change (**Figure 5A and 5B and Figure 5 –**
325 **figures supplement 1A, 1B, 2A, 2B**). The fold change for the T1-TP(3C) levels relative
326 to the T1 was similar to T1-TP(2C)(**Figure 5B and Figure 5 – figures supplement 1B**
327 **and 2B and Table 3**). These data provide further evidence that the GGXXG and
328 (C/F)CV+C motifs together are key determinants of the LCK-independent contributions
329 that CD4 makes to amplifying pMHCII-specific proximal signaling.
330 Finally, the percent responders were lower for pCD3ζ and pZAP70 for T1-TP(3C)
331 compared to WT (**Figure 5 and Figure 5 – figures supplement 1C and 2C**). These
332 data are consistent with the idea that, in the absence of the intracellular domain,

333 mutating these motifs influences initiation of key signaling events. See **Table 3** for a
334 summary of the data.
335
336 **Discussion**
337 Our computational reconstruction of CD4 evolution provided access to a subset of
338 results from experiments that Nature performed over ~435 million years in a greater
339 variety of jawed vertebrates, in the wild, than could be achieved with mouse or human
340 samples in the lab (Lee et al., 2022). It allowed us to identify residues that were
341 selected under purifying selection, and are thus predicted to be functionally significant,
342 because acquiring a mutation at these residues would affect fitness and results in a
343 failure to propagate the change to future progeny. Our structure-function analysis of
344 these residues in 58$\alpha^-\beta^-$ cells, which we continued in this study, provided a second
345 system to cross-validate the functional significance of particular residues and allowed us
346 to start providing mechanistic insights into why these residues are important.
347 The data presented here are not consistent with predictions of the prevailing
348 model in which CD4 recruits LCK to CD3 ITAMs to initiate signaling. Importantly, this
349 study builds upon our prior work by showing that while reducing CD4-LCK interactions
350 reduces pMHCII-specific IL-2 production in our system, either by mutating the CQC
351 clasp or removing the CD4 intracellular domain entirely, this cannot be attributed to
352 reductions in pCD3ζ levels as predicted by the TCR signaling paradigm (Lee et al.,
353 2022). It is notable that, in the absence of CD4-pMHCII interactions (T1$^{\Delta bind}$ mutant),
354 pCD3ζ levels were roughly half of those measured when CD4-pMHCII interactions
355 occurred (T1 mutant). We take these data together as evidence that there is a threshold

356 for the number of phosphorylated CD3ζ molecules, and/or the duration of signaling, that
357 is required to drive IL-2 production in our system. We also conclude that CD4 binding to
358 pMHCII functions to increase the number of TCR-CD3 complexes per cell that
359 experience CD3ζ phosphorylation to reach that threshold and/or sustain signaling.
360 Furthermore, CD4-pMHCII interactions similarly impacts pZAP70 and pPLCγ1 levels,
361 albeit to a lesser extent for the latter.

362 A logical extension of these conclusions is that there is a density of agonist
363 pMHCII below which CD4 binding to pMHCII is essential for signal initiation. This idea is
364 supported by findings that CD4 is necessary for signal propagation and amplification to
365 the calcium mobilization step in response to fewer than 25 agonist pMHCII (Irvine et al.,
366 2002). Attempting to accurately measure the contributions of CD4 to ITAM
367 phosphorylation, with or without mutant motifs, at very low densities of pMHCII would be
368 challenging and is technically beyond the scope of this study. Nevertheless, in this and
369 our prior publication we did not observe the expected decreases in pCD3ζ levels when
370 CD4-LCK interactions were reduced by mutating the CQC clasp motif, the IKRLL motif,
371 or by eliminating the intracellular domain. Furthermore, we found in our prior study that
372 IL-2 production increased significantly when we mutated the full intracellular helix, the
373 helix and CQC clasp together, or the IKRLL motif alone. These direct tests of the TCR
374 signaling paradigm are inconsistent with predictions of the model. As such, they suggest
375 that the contributions of CD4 to signal initiation and amplification at the early timepoint
376 we measured are independent of direct CD4-LCK interactions.

377 Because the combined impact of mutating the GGXXG and (C/F)CV+C motifs
378 reduced pCD3ζ levels to ~16% of the contribution of CD4-pMHCII engagement, even

379 when direct CD4-LCK interactions were absent, we can conclude that the GGXXG and
380 (C/F)CV+C motifs are key determinants that help CD4 drive signaling above the
381 threshold required for IL-2 production. Our data also provide evidence that mutating the
382 GGXXG and (C/F)CV+C motifs together can reduce the frequency of cells experiencing
383 CD3ζ and ZAP70 phosphorylation in the absence of the intracellular domain. Given that
384 palmitoylation is rapidly reversible, these data suggest that the switch-like function of
385 the palmitoylation motif may influence signal initiation. Interestingly, unlike CD4-pMHCII
386 interactions, these motifs are not essential for signaling output at high ligand densities
387 as we observed low levels of IL-2 produced in cells bearing mutants of these motifs with
388 increasing doses of agonist pMHCII. Binding of CD4 and TCR-CD3 to pMHCII can
389 therefore amplify pMHCII-specific signaling without the contributions of the GGXXG and
390 (C/F)CV+C motifs, or motifs in the intracellular domain, albeit at lower levels than if
391 these motifs are intact. This could be due to the contributions of additional unidentified
392 motifs in the transmembrane domain, or to the increase in TCR-CD3 dwell time on
393 pMHCII that is mediated by the CD4 extracellular domain (Glassman et al., 2018).
394 Given that these motifs were essential for IL-2 production at low ligand densities, a
395 logical extension of these data is that there is an agonist pMHCII density below which
396 these motifs are essential for the initiation of early signaling events.
397 The data from our current study indicate that the GGXXG and (C/F)CV+C motifs
398 do not influence early signaling events by regulating the ability of CD4 to either recruit
399 LCK to, or sequester it away from, the TCR-CD3 ITAMs as we previously postulated
400 (Lee et al., 2022). Instead, they work independently of CD4-LCK interactions to
401 enhance pMHCII-specific signaling. It is tempting to speculate that because these motifs

402 can regulate CD4 membrane domain localization and, because in other proteins
403 palmitate moieties can sandwich cholesterol against the flat surface of a GG patch on a
404 transmembrane domain helix, these motifs may allow CD4 to regulate local
405 concentration of cholesterol or cholesterol sulfate around TCR-CD3, perhaps by taking
406 such molecules away from TCR-CD3 to stabilize allosteric changes associated with
407 signaling (Chen et al., 2022; Fessler, 2016; Gil et al., 2002; Lee et al., 2015; Song et al.,
408 2014; Swamy et al., 2016; Teese and Langosch, 2015; Wacker et al., 2013; Wang et
409 al., 2016). These CD4 motifs may also impact the accessibility of ITAMs for LCK
410 phosphorylation by changing the local membrane environment around TCR-CD3 upon
411 reciprocal engagement of pMHCII (Aivazian and Stern, 2000; Xu et al., 2008). Finally, it
412 is worth considering that, in our prior study, we found G402 of the GGXXG motif has
413 covaried over evolutionary time with L438 of the intracellular helix IKRLL motif that has
414 inhibitory function, suggesting that the function of these motifs are co-evolving (Lee et
415 al., 2022). In support of this idea, we reported that the signal enhancing activity of the
416 GGXXG and (C/F)CV+C motifs together counterbalanced the inhibitory activity of the
417 IKRLL motif with regards to IL-2 production. It is unclear at this point if this
418 counterbalancing is simply additive of individual motif functions, or if there is a functional
419 interplay of the motifs when the intracellular domain of CD4 is present. Delineating the
420 mechanistic details by which the GGXXG and (C/F)CV+C motifs increase signaling on
421 their own, or when combined, and how their function integrates with those of other
422 motifs will be the subject of future investigations.
423 Altogether, the data in this and our preceding study provide direct evidence that
424 complement indirect results indicating that pMHCII-specific signaling is not initiated, or

425 dependent on, CD4 recruitment of LCK kinase activity to the CD3 ITAMs (Glassman et
426 al., 2018; Horkova et al., 2023; Killeen and Littman, 1993; Lee et al., 2022; Xu and
427 Littman, 1993). Recent work on CD8 suggest that this coreceptor also does not recruit
428 LCK to phosphorylate CD3 ITAMs (Casas et al., 2014; Wei et al., 2020). In total, these
429 findings suggest that the TCR signaling paradigm needs revising as it pertains to
430 coreceptor-LCK interactions. For CD4, the existing evidence suggest that reciprocal
431 binding of CD4 and TCR-CD3 enables free LCK and FYN to initiate signaling by
432 phosphorylating the ITAMs and ZAP70 (Glassman et al., 2016; Glassman et al., 2018;
433 Horkova et al., 2023; Lee et al., 2022; Salmond et al., 2009; van Oers et al., 1996). The
434 contribution of the current study is in showing the GGXXG and (C/F)CV+C motifs work
435 together to enhance these early signaling events independently of direct CD4-LCK
436 interactions.

437 Finally, it is interesting to consider what the primary purpose of CD4-LCK
438 interactions via the CQC clasp and IKRLL motifs are if not to recruit LCK kinase activity
439 to the CD3 ITAMs. Data from two studies suggest that LCK makes a kinase-
440 independent contribution to pMHCII-specific responses; it is therefore plausible that the
441 phenotype reported for CD4 when the CQC clasp is mutated is due to relieving the
442 kinase-independent scaffolding function of LCK (Horkova et al., 2023; Xu and Littman,
443 1993). In addition, CD4-LCK interaction via the CQC clasp motif and the intracellular
444 helix will prevent the helix from interacting with other partners, thus mutating the CQC
445 clasp would favor helix interactions with other putative partners (Lee et al., 2022).
446 Finally, the CQC clasp is thought to play a role in positioning CD4 in proximity to LAT,
447 either through direct or indirect interactions, which could contribute to the phenotype of

448 CQC clasp mutants (Bosselut et al., 1999; Lo et al., 2018; Lo et al., 2019). If CD4-LCK
449 and CD4-LAT interactions are mutually exclusive, and both require the CQC clasp, then
450 mutating this motif would have a greater impact than just relieving CD4-LCK interactions
451 (Bosselut et al., 1999). These questions remain outstanding, as do questions
452 concerning how the intracellular helix regulates pMHCII-specific signaling.

453 In closing, the broader implications of the data presented in our current and prior
454 evolution-structure-function studies provide fertile ground for future directions beyond
455 those mentioned above. Our approach allows us to identify functionally important
456 residues/motif and then interrogate basic mechanistic principles of their function that
457 should hold true across $CD4^+$ T cell subsets since the biochemical and biophysical
458 bases for interactions between CD4 and its interacting partners (i.e. other proteins or
459 membrane components) should be the same in $58\alpha^-\beta^-$ cells as in thymocytes or in
460 different $CD4^+$ T cells. However, different $CD4^+$ T cell populations will have different
461 levels of expression of relevant proteins (e.g. interacting partners or modifying
462 enzymes), and may even have differences in lipid composition, such that the impact of
463 the motifs we have identified and studied to date may lead to different outcomes in
464 different $CD4^+$ T cell subsets (http://immpres.co.uk/)(Tuosto and Xu, 2018). For
465 example, differences in expression of enzymes with switch-like functions, such as those
466 that add or remove palmitate to the (C/F)CV+C motif, or those that phosphorylate or
467 dephosphorylate the serines in the intracellular helix that regulate CD4-LCK interactions
468 and inhibitory activity, may vary between naïve $CD4^+$ T cells, different Th subsets, or
469 Tregs to differentially tune the activity of these motifs and their impact on pMHCII-
470 specific signaling. Now that we have identified residues and broader motifs that have

471 proven to be functionally important *in vivo* over 435 million years of evolution, while also
472 providing mechanistic insights as to why the residues are important, there is utility in
473 evaluating the impact of mutant CD4 mice on thymocyte development, naïve $CD4^+$ T
474 cell activation and differentiation, and the execution of Th and Treg effector functions. In
475 so doing, we will gain additional insights into why there is a fitness cost if a mutation is
476 acquired in these residues. Such knowledge will increase our fundamental
477 understanding of $CD4^+$ T cell biology and will also be critical for biomimetic engineering
478 of synthetic receptors that can redirect $CD4^+$ T cell activity for therapeutic purposes.
479

480 **MATERIALS AND METHODS**

481 **Evolutionary analyses**

482 Available CD4 orthologs were identified through reciprocal blast-based searches and
483 downloaded from GenBank. BLAST may not only identify orthologs, so additional
484 criteria were used to include putative orthologous CD4 sequences in our analyses:
485 presence of a domain structure consisting of four extracellular Ig domains followed by a
486 transmembrane domain and a C-terminal intracellular domain, including the presence of
487 the LCK binding clasp (CxC). Sequences that were shorter, contained frameshift
488 mutations, or displayed high sequence variability were excluded from the analysis. For
489 the current study, teleost fish were considered to be the oldest living species that
490 contain a CD4 molecule given that a CD4 ortholog was not reported in the elephant
491 shark (*Callorhinchus milii*), although future analyses of other cartilaginous fishes might
492 yield more distant orthologs (Venkatesh et al., 2014). The final dataset contained 99
493 unique CD4 orthologs, ranging from teleost fish to human. These (putative) coding

494 sequences were translated to amino-acids and aligned using MAFFT (Katoh et al.,
495 2002). For codon-based analyses, the aligned amino acid sequences were back
496 translated to nucleotides to maintain codons. The multiple sequence alignments were
497 further processed to remove all insertions (indels) relative to the mouse CD4 sequence
498 (NM_013488.3) to maintain consistent numbering of sites. The 5' and 3' regions of the
499 CD4 molecules were not consistently aligned due to different start codon usage or
500 extensions of the ICD, respectively. The alignment was edited to start at the codon
501 (AAG) coding for K48 within mouse CD4. The alignment that includes all 99 CD4
502 sequences ends at the last cysteine residue that makes up the CQC clasp. For the
503 mammalian only dataset, the alignment terminates at the mouse CD4 stop codon.
504 FastTree was used to estimate maximum likelihood trees (Price et al., 2010). For
505 amino acid-based trees, the Jones-Taylor-Thornton (JTT) model of evolution was
506 selected, while the General Time-Reversible (GTR) model was used for nucleotide trees
507 (Jones et al., 1992; Waddell and Steel, 1997). In all conditions, a discrete gamma model
508 with 20 rate categories was used. A reduced representation tree (based on the amino
509 acid alignment) is shown in Figure 1A. We used the same JTT model to estimate the
510 marginal reconstructions of nodes indicated in Figure 1A. Phylogenetic trees and logo
511 plots were visualized in Geneious and further edited using Adobe Illustrator. Ancestral
512 sequences were estimated using GRASP (Foley et al., 2020).
513 Codon-based analysis of selection was performed using the hypothesis testing
514 fixed effects likelihood (FEL) model as implemented within the phylogenies (HyPhy)
515 package (version 2.5.14) (MP) (Kosakovsky Pond et al., 2020; Pond et al., 2005; Pond
516 and Frost, 2005; Weaver et al., 2018). The back-translated codon-based alignments

517 described above were used for these analyses. FEL uses likelihood ratio tests (LRTs) to
518 assess a better fit of codons that allowed selection ($p < 0.1$). When calculating values for
519 all CD4 orthologs included in the initial phylogenetic analysis we analyzed and identified
520 the sequences within the mammalian clade as the foreground branches on which to test
521 for evolutionary selection in order to maximize statistical power.

522 Covariation between protein residues was calculated using the MISTIC2 server.
523 We calculated 4 different covariation methods (MIp, mFDCA, plmDCA, and
524 gaussianDCA)(Colell et al., 2018). Protein conservation scores were calculated based
525 on the protein alignment using the ConSurf Server (Ashkenazy et al., 2016; Ashkenazy
526 et al., 2010). ConSurf conservation scores are normalized, so that the average score for
527 all residues is zero, with a standard deviation of one. The lower the score, the more
528 conserved the protein position. For the purpose of this study, residues were considered
529 to covary if the MI was larger than 4 and both residues had a ConSurf conservation
530 score lower than -0.5. Also, pairs with an MI larger than 8 were considered to covary if
531 the conservation score was below -0.3. Using these criteria, we selected 0.5% of all
532 possible pairs as recommended (Buslje et al., 2009; Colell et al., 2018).

533 Statistical analyses and associated raw data for the figures are available on
534 Dryad (doi:10.5061/dryad.p8cz8w9vw).

535 **Cell lines**

536 58$\alpha^-\beta^-$ T cell hybridoma lines were generated from Kuhns Lab stocks of parental 58$\alpha^-\beta^-$
537 T cell hybridoma cells (obtained from Y.H. Chien at Stanford University) by retroviral
538 transduction and maintained in culture by standard techniques as previously described
539 (Glassman et al., 2018; Letourneur and Malissen, 1989). 58$\alpha^-\beta^-$ T cell hybridomas lack

540 expression of endogenous TCRα and TCRβ chains, are CD4 negative, make IL-2 in
541 response to TCR signaling, and are variant of the DO-11.10.7 mouse T cell hybridoma
542 (Balb/c T cell fused to BW5147 thymoma)(Letourneur and Malissen, 1989). We validate
543 the cells lines by these characteristics as well as expression of H2-D^d to validate Balb/c
544 origin. In brief, one day after transduction the cells were cultured in 5μg/ml
545 puromycin(Invivogen) and 5μg/ml zeocin(ThermoFisher Scientific) in RPMI 1640
546 (Gibco) supplemented with 5% FBS (Atlanta Biologicals or Omega Scientific), Penicillin-
547 Streptomycin-Glutamine (Cytiva), 10µg/ml Ciprofloxacin (Sigma), and 50µM beta-2-
548 mercaptoethanol (ThermoFisher Scientific). The next day drug concentrations were
549 increased to 10μg/ml puromycin (Invivogen) and 100μg/ml zeocin (ThermoFisher
550 Scientific) in 10ml in a T25 flask. Aliquot of $1x10^7$ cells were frozen at days 5, 7, and 9.
551 Cells were thawed from the day 5 freeze and cultured for 3 days in 10μg/ml puromycin
552 and 100μg/ml zeocin, and maintained below $1x10^6$ cells/ml to use in the functional
553 assays. Cells used in the functional assays were grown to $0.8x10^6$ cells/ml density and
554 replicates of three functional assays were performed every other day. If cells exceeded
555 $1x10^6$ cells/ml at any point in the process they were discarded as they lose reactivity at
556 high cell densities and a new set of vials was thawed. Typically, two independent WT
557 and mutant pairs were generated for any given mutant and tested for IL-2 to gain further
558 confidence in a response phenotype. When cells lines are presented together in a
559 graph, that indicates that the cell lines (WT and mutants sets) were generated at the
560 same time from the same parental cell stock.
561 Given the number of mutant CD4 cell lines generated and handled in this study,
562 the identity of the transduced CD4 gene was verified by PCR sequencing at the

563 conclusion of three independent functional assays. 58$\alpha^-\beta^-$ T cell hybridomas were lysed
564 using DirectPCR Tail Lysis Buffer (Viagen Biotech) with proteinase K (SIGMA) for 2
565 hours at 65˚C. Cells were then heated at 95˚C for ten minutes. Cell debris was pelleted,
566 and the supernatants were saved. CD4 was amplified by PCR using Q5 DNA Hot Start
567 Polymerase (New England BioLabs) in 0.2μM dNTP, 0.2μM primer concentration, Q5
568 Reaction buffer, and water. CD4 was amplified using the following primers:
569 5' primer: acggaattccgctcgagcgccaccatggtgcgagccatctctctcttagg
570 3' primer: ctagcaagcttgtcgactcaagatcttcattagatgagattatggctcttctgc
571 Product were purified using SpinSmart Nucleic Acid Purification Columns (Thomas
572 Scientific) and sent to Eton Bioscience for sequencing with the following 5' CD4 primer:
573 gtctctgaggagcagaag.
574 The I-E^{k+} M12 cells used as antigen presenting cells (APCs) were previously
575 reported (Glassman et al., 2018). M12 cells are a murine B cell lymphoma from Balb/c
576 mice (H2-D^d validated)(Kim et al., 1979). Cells were cultured in RPMI 1640 (Gibco)
577 supplemented with 5% FBS (Atlanta Biologicals or Omega Scientific), Pencillin-
578 Streptomycin-Glutamine (Cytiva), 10μg/ml Ciprofloxacin (Sigma), 50μM beta-2-
579 mercaptoethanol (ThermoFisher Scientific), and 5μg/mL Puromycin (Invivogen) and
580 50μg/ml Zeocin (ThermoFisher). The parental cells are maintained in Kuhns Lab stocks
581 and were originally obtained from MM Davis stocks (Stanford University).
582 Parental 58$\alpha^-\beta^-$ T cell hybridoma and M12 cells are periodically treated with
583 Plasmocyn and tested for mycoplasma contamination by PCR using primer sequences
584 available from ATCC (5' primer sequence: TGCACCATCTGTCACTCTGTTAACCTC; 3'
585 primer sequence: GGGAGCAAACAGGATTAGATACCCT). All transduced cell lines

586 used here were grown in ciprofloxacin and generated from parental cells that had tested
587 negative for mycoplasma.
588 For retroviral production we used Phoenix-eco cells from the Nolan Lab (ATCC
589 CRL-3214).

590 **Antibodies**

Antibodies	Vendor	Catalog number	RRID
anti-mouse CD4 eFlour 450, clone GK1.5	ThermoFisher Scientific	48-0041-82	AB_10718983
anti-mouse TCRα APC, clone RR8-1	ThermoFisher Scientific	17-5800-82	AB_19853170
anti-mouse CD3ε PE-Cy7, clone 145-2C11	ThermoFisher Scientific	25-0031-82	AB_469572
anti-mouse IL-2, clone JES6-1A12	BioLegend	503702	AB_315292
biotin anti-mouse IL-2, clone JES6-5H4	BioLegend	503804	AB_315298
Streptavidin HRP	BioLegend	405210	
anti-mouse TCRβ PE, clone KJ25	BD Pharmingen	553209	AB_394709
biotin anti-mouse CD4 (Clone RM4-4)	BioLegend	116010	AB_2561504
anti-mouse CD4 APC, clone GK1.5	BioLegend	100412	AB_312697
anti-mouse LCK PE, clone 3A5	Santa Cruz	sc-433	
Cholera Toxin Subunit B Alexa Fluor 488	ThermoFisher Scientific	C22841	
anti-mouse pCD3ζ Alexa Flour 647, clone K25-407.69	BD Phosflow	558489	AB_647152
anti-mouse pZAP70 APC, clone n3kobu5	ThermoFisher Scientific	17-9006-42	AB_2573268
anti-mouse pPLCγ1 PE, clone A17025A	BioLegend	612404	AB_2801120

591 **Flow cytometry**

592 Cell surface expression of CD4 and TCR-CD3 complexes were measured by flow
593 cytometry. In brief, cells were stained for 30 minutes at 4ºC in FACS buffer (PBS, 2%
594 FBS, and 0.02% sodium azide) using anti-CD4 (clone GK1.5, eFluor 450 conjugate,

595 ThermoFisher Scientific), anti-TCRα (anti-Vα11, clone RR8-1, APC conjugate,
596 ThermoFisher Scientific), anti-CD3ε (145-2C11, ThermoFisher Scientific) and GFP was
597 detected as a measure of the TCRβ-GFP subunit. Analysis was performed on a Canto II
598 or LSRII (BD Biosciences) at the Flow Cytometry Shared Resource at the University of
599 Arizona. Flow cytometry data were analyzed with FlowJo Version 9 software (Becton,
600 Dickinson & Company).

601 **Functional assays**

602 IL-2 production was measured to quantify pMHCII responses. $5x10^4$ transduced $58\alpha^-\beta^-$
603 T cell hybridomas were cocultured with $1X10^5$ transduced I-E^{k+} M12 cells in triplicate in
604 a 96 well round bottom plate in RPMI with 5% FBS (Omega Scientific), Pen-Strep+L-
605 Glutamine (Cytiva), 10ng/ml ciprofloxacin (Sigma), and 50μM beta-2-mercaptoethanol
606 (Fisher) in the presence of titrating amounts of MCC 88-103 peptide (purchased from
607 21st Century Biochemicals at >95% purity) starting at 30μM MCC and a 1:3 titration
608 (Glassman et al., 2018). For experiments with APCs expressing tethered pMHCII, $5x10^4$
609 $58\alpha^-\beta^-$ T cell hybridomas were cultured with $1X10^5$ MCC:I-E^{k+} or T102S:I-E^{k+} M12 cells
610 in triplicate in a 96 well round bottom plate using the same culture conditions as above.
611 The supernatants were collected and assayed for IL-2 concentration by ELISA after 16
612 hours of co-culture at 37ºC. Anti-mouse IL-2 (clone JES6-1A12, BioLegend) antibody
613 was used to capture IL-2 from the supernatants, and biotin anti-mouse IL-2 (clone
614 JES6-5H4, BioLegend) antibody was used as the secondary antibody. Streptavidin-
615 HRP (BioLegend) and TMB substrate (BioLegend) were also used.

616 To assess engagement-induced endocytosis, CD4 surface levels were measured
617 by flow cytometry 16hrs after coculture with APCs and peptide as described above for

618 IL-2 quantification. 96 well plates containing cells were washed with ice cold FACs
619 buffer (PBS, 2%FBS, 0.02% sodium azide), transferred to ice, and Fc receptors were
620 blocked with Fc block mAb clone 2.4G2 for 15 minutes at 4˚C prior to surface staining
621 for 30 minutes at 4˚C with anti-CD4 (clone GK1.5 EF450, Invitrogen) and anti-Vβ3 TCR
622 clone (clone KJ25, BD Pharmingen) antibodies. Cells were washed with FACS buffer
623 prior to analysis on a LSRII (BD Biosciences) at the Flow Cytometry Shared Resource
624 at the University of Arizona. Flow cytometry data were analyzed with FlowJo Version 10
625 software (Becton, Dickinson & Company). The average of the geometric mean of the
626 TCR or CD4 signal was taken for the triplicate of the post 58$\alpha^-\beta^-$ cells cocultured with
627 M12 I-E^{k+} cells at 0μM MCC concentration. Each value of the raw gMFI of TCR or CD4
628 for cells cultured at 10μM MCC was subtracted from the average gMFI at 0μM. The
629 values show the change of gMFI from 0μM to 10μM.

630 **Sucrose gradient analysis**

631 Membrane fractionation by sucrose gradient was performed similarly to previously
632 described methods (Hur et al., 2003; Parrish et al., 2016). For cell lysis, $6x10^7$ 58$\alpha^-\beta^-$ T
633 cell hybridomas were harvested and washed 2x using TNE buffer (25mM Tris, 150mM
634 NaCl, 5mM EDTA). Cells were lysed on ice in 1% Triton-X detergent in TNE in a total
635 volume of 1mL for 10 minutes and then dounce homogenized 10x. The homogenized
636 lysate was transferred to 14 x 95mm Ultraclear Ultra Centrifuge tubes (Beckman). The
637 dounce homogenizer was rinsed with 1.6mL of the 1% lysis buffer, which was then was
638 added to the Ultracentrifuge tube. 2.5mL of 80% sucrose was added to the centrifuge
639 tube with lysate and mixed well. Gently, 5mL of 30% sucrose was added to the
640 centrifuge tubes, creating a 30% sucrose layer above the ~40% sucrose/lysate mixture.

641 Then, 3mL of 5% sucrose was added gently to the centrifuge tube, creating another
642 layer. The centrifuge tubes were spun 18 hours at 4˚C in a SW40Ti rotor at 36,000rpm.
643 Analysis of membrane fractions was performed via flow-based fluorophore-linked
644 immunosorbent assay (FFLISA) as previously described (Parrish et al., 2016). In brief,
645 88μL of Streptavidin Microspheres 6.0μm (Polysciences) were coated overnight at 4ºC
646 with 8μg of biotinylated anti-CD4 antibody (clone RM4-4, BioLegend). Prior to
647 immunoprecipitation (IP), beads were washed with 10mL of FACS buffer (1x PBS,
648 2%FBS, 0.02% sodium azide) and resuspended in 3.5mL of 0.1% Triton-X 100 lysis
649 wash buffer in TNE. For each cell line lysed, 10 FACS tubes were prepared with 50μL of
650 the washed RM4-4 coated beads. Upon completion of the spin, 500μL was carefully
651 taken off the top of the centrifuge tubes and discarded. Following this, 1mL was
652 extracted from the top of the tube, carefully as to not disrupt the gradient, and added to
653 a FACS tube with coated beads and capped. This was repeated for 10 individual
654 fractions in separate FACS tubes. Following the extraction, lysates were incubated with
655 the beads for 90 minutes, inverting the tubes to mix every 15 minutes.
656 Following the immunoprecipitation, FACS tubes were washed 3x using 0.1%
657 Triton-X lysis wash buffer in TNE. Tubes were then stained using 1μL anti-CD4 (APC
658 conjugate; clone GK1.5, BioLegend), 1.5μL anti-LCK (PE conjugate, clone 3A5, Santa
659 Cruz Biotechnology), and 1μL CTxB (AF 488 conjugate, ThermoFisher Scientific,
660 resuspended as per manufacturer's instructions) for 45 minutes at 4ºC. Following the
661 stain, tubes were washed using 0.1% Triton-X lysis wash buffer in TNE. Analysis of
662 beads were performed on a LSRII (BD Biosciences) at the Flow Cytometry Shared
663 Resource at the University of Arizona. 10^4 events were collected per sample. Flow

664 cytometry data were analyzed with FlowJo Version 10 software (Becton, Dickinson &
665 Company).
666 For FFLISA analysis, raw gMFI values for fraction 1 were subtracted from the
667 rest of the fractions to account for background, such that the gMFI of fraction 1 is 0. To
668 normalize the data, the percentage of CD4 within any given fraction (fx) relative to the
669 total CD4 gMFI (CD4 signal % of total) was calculated by dividing the gMFI signal in a
670 given fraction (fx) by the sum of the total CD4 gMFI signal [sum(f1:f10)CD4 gMFI] and
671 multiplying by 100 [e.g. fx % of total = fx CD4 gMFI / Sum(f1:f10)CD4 gMFI x 100]. To
672 normalize the CTxB and LCK signal in any given fraction relative to the CD4 signal in
673 that same fraction (CTxB or LCK normalized to CD4) the gMFI of CTxB or LCK in fx
674 was divided by the CD4 gMFI of that fx and then multiplied by the percentage of CD4
675 within fx (e.g. Normalized fx LCK = fx LCK gMFI/fx CD4 gMFI x fx CD4% of total CD4
676 gMFI). Area under the curve (AUC) analysis was performed with GraphPad Prism 9 for
677 fractions 1-6 to determine the AUC for the detergent resistant membrane (DRM)
678 domains due to their floating phenotypes, and for fractions 6-10 to determine the AUC
679 for the detergent soluble membrane (DSM) domains.
680 **Intracellular signaling analysis**
681 M12 cells expressing Hb:I-E^k (null) or MCC:I-E^k (cognate) tethered pMHCII complexes
682 were labeled with Tag-it Violet according to the manufacturer's instructions (BioLegend).
683 M12 cells and 58$\alpha^-\beta^-$ cells were then chilled on ice for 30 minutes, $5X10^5$ of each cell
684 type were mixed together in 1.5ml snap cap tubes, and the cells were pelleted at 2000
685 rpm for 30 second at 4°C to force interactions. The supernatant was removed and the
686 tubes were transferred to a 37°C water bath for 2 minutes to enable signaling. Fixation

687 Buffer (BioLegend Inc) was then added for 15 minutes at 37°C. Cells were washed
688 twice with FACs buffer, pelleted at 350xg for 5 minutes at room temperature,
689 resuspended in 1mL True-Phos Perm Buffer (BioLegend Inc), and incubated at -20°C
690 for 16 hours.

691 Cells were blocked with anti-mouse FcRII mAb clone 2.4G2 hybridoma
692 supernatants (ATCC) for 30 minutes, pelleted, and stained on ice for 60 minutes with
693 anti-pCD3ζ (clone K25-407.69, Alexa Fluor 647 conjugate, BD Biosciences) in one
694 sample tube, or with anti-pZAP70 (clone n3kobu5, APC conjugate, Invitrogen) and anti-
695 pPLCγ1 (clone A17025A, PE conjugate, BioLegend) in a separate sample tube at the
696 vendor-recommended concentrations. Finally, cells were washed 2x with FACs buffer at
697 1000xg for 5 minutes at room temperature and analyzed on a Canto II (BD Biosciences)
698 at the Flow Cytometry Shared Resource at the University of Arizona or on a BD
699 Fortessa. $1x10^4$ $58\alpha^-\beta^-$ cell:M12 cell couples were collected per sample.

700 Flow cytometry data were analyzed with FlowJo Verison 10 software (Becton,
701 Dickinson, & Company) by gating on $58\alpha^-\beta^-$ and M12 cell couples, as described
702 previously (Glassman et al., 2018). Histograms of the pCD3ζ, pZAP70, or pPLCγ1
703 intensity for the gated population were then generated and data expressing the gated
704 populations as numbers of cells within intensity bins was exported from FlowJo into
705 Microsoft Excel where the number of cells for each bin intensity value for MCC:I-E^k
706 stimulated cells was subtracted from Hb:I-E^k stimulated cells on a bin-by-bin basis. This
707 allowed us to enumerate the intensity differences per bin upon stimulation with the
708 agonist pMHCII over background. Mean intensity and standard error of the mean (SEM)
709 were calculated based on the background subtracted (MCC:I-E^k-Hb:I-E^k) data. The data

710 was then transferred to Prism 9 where we performed smoothing analysis with 500
711 nearest neighbors to smooth the line profile for graphing purposes. Those intensity bins
712 with positive values were considered to contain cells that had responded to the MCC:I-
713 E^k stimuli above background.

714 **Statistical Analysis**

715 Statistical analyses of sucrose gradient and functional assays were performed with
716 GraphPad Prism 9 software as indicated in the figure legends. For each functional
717 assay (IL-2 production and CD4 endocytosis), each individual experiment (biological
718 replicate) was performed with triplicate analysis (technical replicates) and each
719 experiment was repeated three times (3 biological replicates). For sucrose gradient
720 analysis, 10^4 beads were collected by flow cytometry in each experiment (technical
721 replicates) and each experiment was performed three times (biological replicates).
722 Three biological replicates were chosen for each analysis as per convention, and no
723 power calculations were determined. One-Way ANOVA was performed with a Dunnett's
724 posttest when all mutants tested in an experiment were compared to a control sample
725 (e.g. WT). Sidak's posttest were applied when comparing between two specific
726 samples. These posttests were chosen based on Prism recommendations. Student's
727 unpaired t-tests (two-tailed) were performed when comparing WT and LL mutant
728 samples only for phosphorylation analysis.

729 **Constructs**

730 The sequences of 5cc7α, 5cc7βG, CD4 WT and CD4 T1 constructs were previously
731 described (Lee et al., 2022). Full-length CD3δ, ε, γ, and ζ were encoded on a poly-
732 cistronic construct as previously described (Holst et al., 2008; Kuhns and Davis, 2007).

733 The following CD4-T1 constructs: T1-TMD, T1-Palm (2C), T1-Palm (3C), T1-TP (2C),
734 and T1-TP(3C) were cloned by conventional molecular biology techniques, including
735 PCR-based mutagenesis where needed, into pUC18 via 5' EcoRI and 3' HindIII. After
736 sequence verification they were subcloned into pP2 puromycin-resistance MSCV vector
737 (MCS-IRES-puro) via 5' XhoI and 3' BglII, midi-prepped (Qiagen), and sequence
738 verified. Mutated codons are shown in bold uppercase letters, while the motif under
739 interrogation is shown in bold and underlined (any non-mutated codons within the motif
740 are bold lowercase letters and underlined). The sequences for these constructs are as
741 follows:

742 **T1-TMD**:
743 acggaattccgctcgagcgccaccatggtgcgagccatctctcttaggcgcttgctgctgctgctgctgcagctgtcacaac
744 tcctagctgtcactcaagggaagacgctggtgctggggaaggaaggggaatcagcagaactgccctgcgagagttccc
745 agaagaagatcacagtcttcacctggaagttctctgaccagaggaagattctggggcagcatggcaaaggtgtattaatta
746 gaggaggttcgccttcgcagtttgatcgttttgattccaaaaaaggggcatgggagaaaggatcgtttcctctcatcatcaat
747 aaacttaagatggaagactctcagacttatatctgtgagctggagaacaggaaagaggaggtggagttgtgggtgttcaa
748 agtgaccttcagtccgggtaccagcctgttgcaagggcagagcctgaccctgaccttggatagcaactctaaggtctctaa
749 ccccttgacagagtgcaaacacaaaaagggtaaagttgtcagtggttccaaagttctctccatgtccaacctaagggttca
750 ggacagcgacttctggaactgcaccgtgaccctggaccagaaaaagaactggttcggcatgacactctcagtgctgggtt
751 ttcagagcacagctatcacggcctataagagtgagggagagtcagcggagttctccttcccactcaactttgcagaggaa
752 aacgggtggggagagctgatgtggaaggcagagaaggattctttcttccagccctggatctccttctccataaagaacaa
753 agaggtgtccgtacaaaagtccaccaaagacctcaagctccagctgaaggaaacgctcccactcaccctcaagatacc
754 ccaggtctcgcttcagtttgctggttctggcaacctgactctgactctggacaaagggacactgcatcaggaagtgaacctg
755 gtggtgatgaaagtggctcagctcaacaatactttgacctgtgaggtgatgggacctacctctcccaagatgagactgacc
756 ctgaagcaggagaaccaggaggccagggtctctgaggagcagaaagtagttcaagtggtggcccctgagacagggct
757 gtggcagtgtctactgagtgaaggtgataaggtcaagatggactccaggatccaggttttatccagaggggtgaaccaga
758 cagtgttcctggcttgcgtgctg**ggtGTGtccttcCTC**tttctgggtttccttgggctctgcatcctctgctgtgtcaggtgcc
759 ggtgataaagatcttgagtcgacaagcttgctag
760
761 **T1-Palm (2C)**:
762 acggaattccgctcgagcgccaccatggtgcgagccatctctcttaggcgcttgctgctgctgctgctgcagctgtcacaac
763 tcctagctgtcactcaagggaagacgctggtgctggggaaggaaggggaatcagcagaactgccctgcgagagttccc
764 agaagaagatcacagtcttcacctggaagttctctgaccagaggaagattctggggcagcatggcaaaggtgtattaatta
765 gaggaggttcgccttcgcagtttgatcgttttgattccaaaaaaggggcatgggagaaaggatcgtttcctctcatcatcaat
766 aaacttaagatggaagactctcagacttatatctgtgagctggagaacaggaaagaggaggtggagttgtgggtgttcaa
767 agtgaccttcagtccgggtaccagcctgttgcaagggcagagcctgaccctgaccttggatagcaactctaaggtctctaa
768 ccccttgacagagtgcaaacacaaaaagggtaaagttgtcagtggttccaaagttctctccatgtccaacctaagggttca

769 ggacagcgacttctggaactgcaccgtgaccctggaccagaaaaagaactggttcggcatgacactctcagtgctgggtt
770 ttcagagcacagctatcacggcctataagagtgagggagagtcagcggagttctccttcccactcaactttgcagaggaa
771 aacgggtggggagagctgatgtggaaggcagagaaggattctttcttccagccctggatctccttctccataaagaacaa
772 agaggtgtccgtacaaaagtccaccaaagacctcaagctccagctgaaggaaacgctcccactcaccctcaagatacc
773 ccaggtctcgcttcagtttgctggttctggcaacctgactctgactctggacaaagggacactgcatcaggaagtgaacctg
774 gtggtgatgaaagtggctcagctcaacaatactttgacctgtgaggtgatgggacctacctctcccaagatgagactgacc
775 ctgaagcaggagaaccaggaggccagggtctctgaggagcagaaagtagttcaagtggtggcccctgagacagggct
776 gtggcagtgtctactgagtgaaggtgataaggtcaagatggactccaggatccaggttttatccagaggggtgaaccaga
777 cagtgttcctggcttgcgtgctgggtggctccttcggctttctgggtttccttgggctctgcatcctc**tgcTCTgtcaggTCC**
778 **cgg**tgataaagatcttgagtcgacaagcttgctag
779
780 **T1-Palm (3C)**:
781 acggaattccgctcgagcgccaccatggtgcgagccatctctcttaggcgcttgctgctgctgctgctgcagctgtcacaac
782 tcctagctgtcactcaagggaagacgctggtgctggggaaggaaggggaatcagcagaactgccctgcgagagttccc
783 agaagaagatcacagtcttcacctggaagttctctgaccagaggaagattctggggcagcatggcaaaggtgtattaatta
784 gaggaggttcgccttcgcagtttgatcgttttgattccaaaaaaggggcatgggagaaaggatcgtttcctctcatcatcaat
785 aaacttaagatggaagactctcagacttatatctgtgagctggagaacaggaaagaggaggtggagttgtgggtgttcaa
786 agtgaccttcagtccgggtaccagcctgttgcaagggcagagcctgaccctgaccttggatagcaactctaaggtctctaa
787 ccccttgacagagtgcaaacacaaaaagggtaaagttgtcagtggttccaaagttctctccatgtccaacctaagggttca
788 ggacagcgacttctggaactgcaccgtgaccctggaccagaaaaagaactggttcggcatgacactctcagtgctgggtt
789 ttcagagcacagctatcacggcctataagagtgagggagagtcagcggagttctccttcccactcaactttgcagaggaa
790 aacgggtggggagagctgatgtggaaggcagagaaggattctttcttccagccctggatctccttctccataaagaacaa
791 agaggtgtccgtacaaaagtccaccaaagacctcaagctccagctgaaggaaacgctcccactcaccctcaagatacc
792 ccaggtctcgcttcagtttgctggttctggcaacctgactctgactctggacaaagggacactgcatcaggaagtgaacctg
793 gtggtgatgaaagtggctcagctcaacaatactttgacctgtgaggtgatgggacctacctctcccaagatgagactgacc
794 ctgaagcaggagaaccaggaggccagggtctctgaggagcagaaagtagttcaagtggtggcccctgagacagggct
795 gtggcagtgtctactgagtgaaggtgataaggtcaagatggactccaggatccaggttttatccagaggggtgaaccaga
796 cagtgttcctggcttgcgtgctgggtggctccttcggctttctgggtttccttgggctctgcatcctc**TCCTCTgtcaggTC**
797 **Ccgg**tgataaagatcttgagtcgacaagcttgctag
798
799 **T1-TP (2C)**:
800 acggaattccgctcgagcgccaccatggtgcgagccatctctcttaggcgcttgctgctgctgctgctgcagctgtcacaac
801 tcctagctgtcactcaagggaagacgctggtgctggggaaggaaggggaatcagcagaactgccctgcgagagttccc
802 agaagaagatcacagtcttcacctggaagttctctgaccagaggaagattctggggcagcatggcaaaggtgtattaatta
803 gaggaggttcgccttcgcagtttgatcgttttgattccaaaaaaggggcatgggagaaaggatcgtttcctctcatcatcaat
804 aaacttaagatggaagactctcagacttatatctgtgagctggagaacaggaaagaggaggtggagttgtgggtgttcaa
805 agtgaccttcagtccgggtaccagcctgttgcaagggcagagcctgaccctgaccttggatagcaactctaaggtctctaa
806 ccccttgacagagtgcaaacacaaaaagggtaaagttgtcagtggttccaaagttctctccatgtccaacctaagggttca
807 ggacagcgacttctggaactgcaccgtgaccctggaccagaaaaagaactggttcggcatgacactctcagtgctgggtt
808 ttcagagcacagctatcacggcctataagagtgagggagagtcagcggagttctccttcccactcaactttgcagaggaa
809 aacgggtggggagagctgatgtggaaggcagagaaggattctttcttccagccctggatctccttctccataaagaacaa
810 agaggtgtccgtacaaaagtccaccaaagacctcaagctccagctgaaggaaacgctcccactcaccctcaagatacc
811 ccaggtctcgcttcagtttgctggttctggcaacctgactctgactctggacaaagggacactgcatcaggaagtgaacctg
812 gtggtgatgaaagtggctcagctcaacaatactttgacctgtgaggtgatgggacctacctctcccaagatgagactgacc
813 ctgaagcaggagaaccaggaggccagggtctctgaggagcagaaagtagttcaagtggtggcccctgagacagggct
814 gtggcagtgtctactgagtgaaggtgataaggtcaagatggactccaggatccaggttttatccagaggggtgaaccaga

cagtgttcctggcttgcgtgctg**ggtGTGtccttcCTC**tttctgggtttccttgggctctgcatcctc**tgcTCTgtcaggTCCcgg**tgataaagatcttgagtcgacaagcttgctag

T1-TP (3C):
acggaattccgctcgagcgccaccatggtgcgagccatctctcttaggcgcttgctgctgctgctgctgcagctgtcacaac
tcctagctgtcactcaagggaagacgctggtgctggggaaggaaggggaatcagcagaactgccctgcgagagttccc
agaagaagatcacagtcttcacctggaagttctctgaccagaggaagattctggggcagcatggcaaaggtgtattaatta
gaggaggttcgccttcgcagtttgatcgttttgattccaaaaaaggggcatgggagaaaggatcgtttcctctcatcatcaat
aaacttaagatggaagactctcagacttatatctgtgagctggagaacaggaaagaggaggtggagttgtgggtgttcaa
agtgaccttcagtccgggtaccagcctgttgcaagggcagagcctgaccctgaccttggatagcaactctaaggtctctaa
ccccttgacagagtgcaaacacaaaaagggtaaagttgtcagtggttccaaagttctctccatgtccaacctaagggttca
ggacagcgacttctggaactgcaccgtgaccctggaccagaaaaagaactggttcggcatgacactctcagtgctgggtt
ttcagagcacagctatcacggcctataagagtgagggagagtcagcggagttctccttcccactcaactttgcagaggaa
aacgggtggggagagctgatgtggaaggcagagaaggattctttcttccagccctggatctccttctccataaagaacaa
agaggtgtccgtacaaaagtccaccaaagacctcaagctccagctgaaggaaacgctcccactcaccctcaagatacc
ccaggtctcgcttcagtttgctggttctggcaacctgactctgactctggacaaagggacactgcatcaggaagtgaacctg
gtggtgatgaaagtggctcagctcaacaatactttgacctgtgaggtgatgggacctacctctcccaagatgagactgacc
ctgaagcaggagaaccaggaggccagggtctctgaggagcagaaagtagttcaagtggtggcccctgagacagggct
gtggcagtgtctactgagtgaaggtgataaggtcaagatggactccaggatccaggttttatccagaggggtgaaccaga
cagtgttcctggcttgcgtgctg**ggtGTGtccttcCTC**tttctgggtttccttgggctctgcatcctc**TCCTCTgtcaggTCCcgg**tgataaagatcttgagtcgacaagcttgctag

The gene of T1$^{\Delta bind}$ was made by cloning the in frame extracellular domain of CD4 that encodes the Δbind extracellular domain (Parrish et al., 2015) flanked by XhoI and BamHI into the T1 gene. The gene was sequence verified in pUC 18, subcloned into pP2 puromycin-resistance MSCV vector (MCS-IRES-puro) via 5' XhoI and 3' BglII, midi-prepped, and sequence verified. The sequence for the construct is as follows with mutated codons shown in bold uppercase letters, while the motif under interrogation is shown in bold and underlined (any non-mutated codons within the motif are bold lowercase letters and underlined):

T1$^{\Delta bind}$:
acggaattccgctcgagcgccaccatggtgcgagccatctctcttaggcgcttgctgctgctgctgctgcagctgtcacaac
tcctagctgtcactcaagggaagacgctggtgctggggaaggaaggggaatcagcagaactgccctgcgagagttccc
agaagaagatcacagtcttcacctggaagttctctgaccagaggaagattctggggcagcatggc**GATggtGATTCAGATAGC**ggaggttcgccttcgcagtttgatcgttttgattccaaaaaaggggcatgggagaaaggatcgtttcctctc
atcatcaataaacttaagatggaagactctcagacttatatctgtgagctggagaacaggaaagaggaggtggagttgtg
ggtgttcaaagtgaccttcagtccgggtaccagcctgttgcaagggcagagcctgaccctgaccttggatagcaactctaa
ggtctctaaccccttgacagagtgcaaacacaaaaagggtaaagttgtcagtggttccaaagttctctccatgtccaaccta
agggttcaggacagcgacttctggaactgcaccgtgaccctggaccagaaaaagaactggttcggcatgacactctcag
tgctgggttttcagagcacagctatcacggcctataagagtgagggagagtcagcggagttctccttcccactcaactttgc
agaggaaaacgggtggggagagctgatgtggaaggcagagaaggattctttcttccagccctggatctccttctccataa
agaacaaagaggtgtccgtacaaaagtccaccaaagacctcaagctccagctgaaggaaacgctcccactcaccctc
aagataccccaggtctcgcttcagtttgctggttctggcaacctgactctgactctggacaaagggacactgcatcaggaa
gtgaacctggtggtgatgaaagtggctcagctcaacaatactttgacctgtgaggtgatgggacctacctctcccaagatg
agactgaccctgaagcaggagaaccaggaggccagggtctctgaggagcagaaagtagttcaagtggtggcccctga

859 gacagggctgtggcagtgtctactgagtgaaggtgataaggtcaagatggactccaggatccaggttttatccagagggg
860 tgaaccagacagtgttcctggcttgcgtgctgggtggctccttcggctttctgggtttccttgggctctgcatcctctgctgtgtca
861 ggtgccggtgataaagatcttgagtcgacaagcttgctag
862

863 **References**
864

865 Aivazian, D., and Stern, L.J. (2000). Phosphorylation of T cell receptor zeta is regulated
866 by a lipid dependent folding transition. Nat Struct Biol *7*, 1023-1026.

867 Ashkenazy, H., Abadi, S., Martz, E., Chay, O., Mayrose, I., Pupko, T., and Ben-Tal, N.
868 (2016). ConSurf 2016: an improved methodology to estimate and visualize evolutionary
869 conservation in macromolecules. Nucleic Acids Res *44*, W344-350.

870 Ashkenazy, H., Erez, E., Martz, E., Pupko, T., and Ben-Tal, N. (2010). ConSurf 2010:
871 calculating evolutionary conservation in sequence and structure of proteins and nucleic
872 acids. Nucleic Acids Res *38*, W529-533.

873 Bosselut, R., Zhang, W., Ashe, J.M., Kopacz, J.L., Samelson, L.E., and Singer, A.
874 (1999). Association of the adaptor molecule LAT with CD4 and CD8 coreceptors
875 identifies a new coreceptor function in T cell receptor signal transduction. J Exp Med
876 *190*, 1517-1526.

877 Buslje, C.M., Santos, J., Delfino, J.M., and Nielsen, M. (2009). Correction for phylogeny,
878 small number of observations and data redundancy improves the identification of
879 coevolving amino acid pairs using mutual information. Bioinformatics *25*, 1125-1131.

880 Casas, J., Brzostek, J., Zarnitsyna, V.I., Hong, J.S., Wei, Q., Hoerter, J.A., Fu, G.,
881 Ampudia, J., Zamoyska, R., Zhu, C., and Gascoigne, N.R. (2014). Ligand-engaged TCR
882 is triggered by LCK not associated with CD8 coreceptor. Nat Commun *5*, 5624.

883 Chen, Y., Zhu, Y., Li, X., Gao, W., Zhen, Z., Dong, Huang, B., Ma, Z., Zhang, A., Song,
884 X.*, et al.* (2022). Cholesterol inhibits TCR signaling by directly restricting TCR-CD3 core
885 tunnel motility. Mol Cell.

886 Colell, E.A., Iserte, J.A., Simonetti, F.L., and Marino-Buslje, C. (2018). MISTIC2:
887 comprehensive server to study coevolution in protein families. Nucleic Acids Res *46*,
888 W323-W328.

889 Fessler, M.B. (2016). The Intracellular Cholesterol Landscape: Dynamic Integrator of
890 the Immune Response. Trends Immunol *37*, 819-830.

891 Foley, G., Mora, A., Ross, C.M., Bottoms, S., Sützl, L., Lamprecht, M.L., Zaugg, J.,
892 Essebier, A., Balderson, B., Newell, R.*, et al.* (2020). Identifying and engineering
893 ancient variants of enzymes using Graphical Representation of Ancestral Sequence
894 Predictions (GRASP). bioRxiv, 2019.2012.2030.891457.

895 Gil, D., Schamel, W.W., Montoya, M., Sanchez-Madrid, F., and Alarcon, B. (2002).
896 Recruitment of Nck by CD3 epsilon reveals a ligand-induced conformational change
897 essential for T cell receptor signaling and synapse formation. Cell *109*, 901-912.

898 Glaichenhaus, N., Shastri, N., Littman, D.R., and Turner, J.M. (1991). Requirement for
899 association of p56LCK with CD4 in antigen-specific signal transduction in T cells. Cell
900 *64*, 511-520.

901 Glassman, C.R., Parrish, H.L., Deshpande, N.R., and Kuhns, M.S. (2016). The CD4
902 and CD3deltaepsilon Cytosolic Juxtamembrane Regions Are Proximal within a Compact
903 TCR-CD3-pMHC-CD4 Macrocomplex. J Immunol *196*, 4713-4722.

904 Glassman, C.R., Parrish, H.L., Lee, M.S., and Kuhns, M.S. (2018). Reciprocal TCR-
905 CD3 and CD4 Engagement of a Nucleating pMHCII Stabilizes a Functional Receptor
906 Macrocomplex. Cell Rep *22*, 1263-1275.

907 Harris, D.T., and Kranz, D.M. (2016). Adoptive T Cell Therapies: A Comparison of T
908 Cell Receptors and Chimeric Antigen Receptors. Trends Pharmacol Sci *37*, 220-230.

909 Holst, J., Wang, H., Eder, K.D., Workman, C.J., Boyd, K.L., Baquet, Z., Singh, H.,
910 Forbes, K., Chruscinski, A., Smeyne, R.*, et al.* (2008). Scalable signaling mediated by T
911 cell antigen receptor-CD3 ITAMs ensures effective negative selection and prevents
912 autoimmunity. Nat Immunol *9*, 658-666.

913 Horkova, V., Drobek, A., Paprckova, D., Niederlova, V., Prasai, A., Uleri, V., Glatzova,
914 D., Kraller, M., Cesnekova, M., Janusova, S.*, et al.* (2023). Unique roles of co-receptor-
915 bound LCK in helper and cytotoxic T cells. Nat Immunol *24*, 174-185.

916 Hur, E.M., Son, M., Lee, O.H., Choi, Y.B., Park, C., Lee, H., and Yun, Y. (2003). LIME,
917 a novel transmembrane adaptor protein, associates with p56LCK and mediates T cell
918 activation. J Exp Med *198*, 1463-1473.

919 Huse, M., Eck, M.J., and Harrison, S.C. (1998). A Zn2+ ion links the cytoplasmic tail of
920 CD4 and the N-terminal region of LCK. J Biol Chem *273*, 18729-18733.

921 Irvine, D.J., Purbhoo, M.A., Krogsgaard, M., and Davis, M.M. (2002). Direct observation
922 of ligand recognition by T cells. Nature *419*, 845-849.

923 Jones, D.T., Taylor, W.R., and Thornton, J.M. (1992). The rapid generation of mutation
924 data matrices from protein sequences. Comput Appl Biosci *8*, 275-282.

925 Katoh, K., Misawa, K., Kuma, K., and Miyata, T. (2002). MAFFT: a novel method for
926 rapid multiple sequence alignment based on fast Fourier transform. Nucleic Acids Res
927 *30*, 3059-3066.

928 Killeen, N., and Littman, D.R. (1993). Helper T-cell development in the absence of CD4-
929 p56LCK association. Nature *364*, 729-732.

930 Kim, K.J., Kanellopoulos-Langevin, C., Merwin, R.M., Sachs, D.H., and Asofsky, R.
931 (1979). Establishment and characterization of BALB/c lymphoma lines with B cell
932 properties. J Immunol *122*, 549-554.

933 Kim, P.W., Sun, Z.Y., Blacklow, S.C., Wagner, G., and Eck, M.J. (2003). A zinc clasp
934 structure tethers LCK to T cell coreceptors CD4 and CD8. Science *301*, 1725-1728.

935 Kobayashi, S., Thelin, M.A., Parrish, H.L., Deshpande, N.R., Lee, M.S., Karimzadeh, A.,
936 Niewczas, M.A., Serwold, T., and Kuhns, M.S. (2020). A biomimetic five-module
937 chimeric antigen receptor ((5M)CAR) designed to target and eliminate antigen-specific T
938 cells. Proc Natl Acad Sci U S A *117*, 28950-28959.

939 Kosakovsky Pond, S.L., Poon, A.F.Y., Velazquez, R., Weaver, S., Hepler, N.L., Murrell,
940 B., Shank, S.D., Magalis, B.R., Bouvier, D., Nekrutenko, A.*, et al.* (2020). HyPhy 2.5-A
941 Customizable Platform for Evolutionary Hypothesis Testing Using Phylogenies. Mol Biol
942 Evol *37*, 295-299.

943 Kuhns, M.S., and Badgandi, H.B. (2012). Piecing together the family portrait of TCR-
944 CD3 complexes. Immunol Rev *250*, 120-143.

945 Kuhns, M.S., and Davis, M.M. (2007). Disruption of extracellular interactions impairs T
946 cell receptor-CD3 complex stability and signaling. Immunity *26*, 357-369.

947 Kuhns, M.S., and Davis, M.M. (2012). TCR Signaling Emerges from the Sum of Many
948 Parts. Frontiers in immunology *3*, 159.

949 Lee, M.S., Glassman, C.R., Deshpande, N.R., Badgandi, H.B., Parrish, H.L.,
950 Uttamapinant, C., Stawski, P.S., Ting, A.Y., and Kuhns, M.S. (2015). A Mechanical
951 Switch Couples T Cell Receptor Triggering to the Cytoplasmic Juxtamembrane Regions
952 of CD3zetazeta. Immunity *43*, 227-239.

953 Lee, M.S., Tuohy, P.J., Kim, C.Y., Lichauco, K., Parrish, H.L., Van Doorslaer, K., and
954 Kuhns, M.S. (2022). Enhancing and inhibitory motifs regulate CD4 activity. eLife *11*,
955 e79508.

956 Letourneur, F., and Malissen, B. (1989). Derivation of a T cell hybridoma variant
957 deprived of functional T cell receptor alpha and beta chain transcripts reveals a
958 nonfunctional alpha-mRNA of BW5147 origin. Eur J Immunol *19*, 2269-2274.

959 Lo, W.L., Shah, N.H., Ahsan, N., Horkova, V., Stepanek, O., Salomon, A.R., Kuriyan, J.,
960 and Weiss, A. (2018). LCK promotes ZAP70-dependent LAT phosphorylation by
961 bridging ZAP70 to LAT. Nat Immunol *19*, 733-741.

962 Lo, W.L., Shah, N.H., Rubin, S.A., Zhang, W., Horkova, V., Fallahee, I.R., Stepanek, O.,
963 Zon, L.I., Kuriyan, J., and Weiss, A. (2019). Slow phosphorylation of a tyrosine residue
964 in LAT optimizes T cell ligand discrimination. Nat Immunol *20*, 1481-1493.

965 Melenhorst, J.J., Chen, G.M., Wang, M., Porter, D.L., Chen, C., Collins, M.A., Gao, P.,
966 Bandyopadhyay, S., Sun, H., Zhao, Z.*, et al.* (2022). Decade-long leukaemia remissions
967 with persistence of CD4(+) CAR T cells. Nature *602*, 503-509.

968 Parrish, H.L., Deshpande, N.R., Vasic, J., and Kuhns, M.S. (2016). Functional evidence
969 for TCR-intrinsic specificity for MHCII. Proc Natl Acad Sci U S A.

970 Parrish, H.L., Glassman, C.R., Keenen, M.M., Deshpande, N.R., Bronnimann, M.P., and
971 Kuhns, M.S. (2015). A Transmembrane Domain GGxxG Motif in CD4 Contributes to Its
972 LCK-Independent Function but Does Not Mediate CD4 Dimerization. PLoS One *10*,
973 e0132333.

974 Pike, L.J. (2006). Rafts defined: a report on the Keystone Symposium on Lipid Rafts
975 and Cell Function. J Lipid Res *47*, 1597-1598.

976 Pond, S.L., Frost, S.D., and Muse, S.V. (2005). HyPhy: hypothesis testing using
977 phylogenies. Bioinformatics *21*, 676-679.

978 Pond, S.L.K., and Frost, S.D.W. (2005). Not so different after all: A comparison of
979 methods for detecting amino acid sites under selection. Mol Biol Evol *22*, 1208-1222.

980 Price, M.N., Dehal, P.S., and Arkin, A.P. (2010). FastTree 2--approximately maximum-
981 likelihood trees for large alignments. PLoS One *5*, e9490.

982 Rabinowitz, J.D., Beeson, C., Lyons, D.S., Davis, M.M., and McConnell, H.M. (1996).
983 Kinetic discrimination in T-cell activation. Proc Natl Acad Sci U S A *93*, 1401-1405.

984 Rudd, C.E. (2021). How the Discovery of the CD4/CD8-p56(LCK) Complexes Changed
985 Immunology and Immunotherapy. Front Cell Dev Biol *9*, 626095.

986 Salmond, R.J., Filby, A., Qureshi, I., Caserta, S., and Zamoyska, R. (2009). T-cell
987 receptor proximal signaling via the Src-family kinases, LCK and Fyn, influences T-cell
988 activation, differentiation, and tolerance. Immunol Rev *228*, 9-22.

989 Song, Y., Kenworthy, A.K., and Sanders, C.R. (2014). Cholesterol as a co-solvent and a
990 ligand for membrane proteins. Protein Sci *23*, 1-22.

991 Swamy, M., Beck-Garcia, K., Beck-Garcia, E., Hartl, F.A., Morath, A., Yousefi, O.S.,
992 Dopfer, E.P., Molnar, E., Schulze, A.K., Blanco, R.*, et al.* (2016). A Cholesterol-Based
993 Allostery Model of T Cell Receptor Phosphorylation. Immunity *44*, 1091-1101.

994 Teese, M.G., and Langosch, D. (2015). Role of GxxxG Motifs in Transmembrane
995 Domain Interactions. Biochemistry *54*, 5125-5135.

996 Tuosto, L., and Xu, C. (2018). Editorial: Membrane Lipids in T Cell Functions. Frontiers
997 in immunology *9*, 1608.

998 van Oers, N.S., Lowin-Kropf, B., Finlay, D., Connolly, K., and Weiss, A. (1996). alpha
999 beta T cell development is abolished in mice lacking both LCK and Fyn protein tyrosine
1000 kinases. Immunity *5*, 429-436.

1001 Venkatesh, B., Lee, A.P., Ravi, V., Maurya, A.K., Lian, M.M., Swann, J.B., Ohta, Y.,
1002 Flajnik, M.F., Sutoh, Y., Kasahara, M.*, et al.* (2014). Elephant shark genome provides
1003 unique insights into gnathostome evolution. Nature *505*, 174-179.

1004 Wacker, D., Wang, C., Katritch, V., Han, G.W., Huang, X.P., Vardy, E., McCorvy, J.D.,
1005 Jiang, Y., Chu, M., Siu, F.Y.*, et al.* (2013). Structural features for functional selectivity at
1006 serotonin receptors. Science *340*, 615-619.

1007 Waddell, P.J., and Steel, M.A. (1997). General time-reversible distances with unequal
1008 rates across sites: mixing gamma and inverse Gaussian distributions with invariant
1009 sites. Mol Phylogenet Evol *8*, 398-414.

1010 Wang, F., Beck-Garcia, K., Zorzin, C., Schamel, W.W., and Davis, M.M. (2016).
1011 Inhibition of T cell receptor signaling by cholesterol sulfate, a naturally occurring
1012 derivative of membrane cholesterol. Nat Immunol *17*, 844-850.

1013 Weaver, S., Shank, S.D., Spielman, S.J., Li, M., Muse, S.V., and Kosakovsky Pond,
1014 S.L. (2018). Datamonkey 2.0: A Modern Web Application for Characterizing Selective
1015 and Other Evolutionary Processes. Mol Biol Evol *35*, 773-777.

1016 Wei, Q., Brzostek, J., Sankaran, S., Casas, J., Hew, L.S., Yap, J., Zhao, X., Wojciech,
1017 L., and Gascoigne, N.R.J. (2020). LCK bound to coreceptor is less active than free LCK.
1018 Proc Natl Acad Sci U S A *117*, 15809-15817.

1019 Wu, L., Wei, Q., Brzostek, J., and Gascoigne, N.R.J. (2020). Signaling from T cell
1020 receptors (TCRs) and chimeric antigen receptors (CARs) on T cells. Cell Mol Immunol
1021 *17*, 600-612.

1022 Xu, C., Gagnon, E., Call, M.E., Schnell, J.R., Schwieters, C.D., Carman, C.V., Chou,
1023 J.J., and Wucherpfennig, K.W. (2008). Regulation of T cell receptor activation by
1024 dynamic membrane binding of the CD3epsilon cytoplasmic tyrosine-based motif. Cell
1025 *135*, 702-713.

1026 Xu, H., and Littman, D.R. (1993). A kinase-independent function of LCK in potentiating
1027 antigen-specific T cell activation. Cell *74*, 633-643.
1028
1029

Figure Legends

Figure 1. Computational reconstruction of CD4 evolution.
The maximum likelihood phylogenetic tree clusters mammalian CD4 sequences. The tree highlights ancestral reconstructions of CD4 sequences from marsupials (kangaroo silhouette), Atlantogenata (elephant), and Boreoeutheria (wildcat). The logoplot of extant eutherian (Atlantogenata and Boreoeutheria) CD4 sequences show sequence conservation over evolutionary time. In these plots, the height of symbols indicates the relative frequency of each amino acid at that specific position. The mouse CD4 numbering (uniprot) is used as a reference, and residues are color-coded based on sidechain polarity. Evolutionary insertion or deletion events are indicated by dashes (-). Most recent common ancestor (MRCA) sequences are shown at each node in the tree (Node 1-4). As in our previous study (Lee et al., 2022), the ratio of synonymous (dS) and nonsynonymous (dN) substitution rates was calculated. Black dots indicate dN/dS ratios that are significantly below 1 across the entire dataset. Red dots indicate residues under purifying selection in the mammalian only dataset. Previously identified motifs are indicated by boxes, while the intracellular domain helix is shaded gray. The arrow at position 422 indicates where CD4 was truncated (CD4-T1), while TMD and T1-Palm show the mutations studied in this study.

Figure 2. Truncating CD4 does not reduce CD3ζ phosphorylation.
(**A**) Representative IL-2 production is shown in response to a titration of MCC peptide from one experiment (left). Experiments were performed in triplicate and each symbol equals the mean +/- SEM at that peptide concentration. AUC analysis for the dose response is shown as a measure of the response magnitude for the average of three independent experiments performed with one independently generated set of cell lines (center). The average response to a low dose (41nM) of peptide is shown as a measure of sensitivity for three independent experiments performed with one independently generated set of cell lines (right). The data are representative of those obtained with 4 (WT vs T1) or 2 (WT vs T1$^{\Delta bind}$) independently generated sets of cell lines.
(**B**) Phosphorylation intensity of CD3ζ (pCD3ζ) for WT and CD4-T1 (T1) (left), normalized pCD3ζ intensity for WT and T1 (center), and average % responders of pCD3ζ for WT and T1 (right). Five independently generated cell lines (biological replicates) were tested for WT and T1. For phosphorylation intensity, each pair of lines (connected symbols) was tested in three independent experiments. Data were analyzed and collected as in Figure 2 – figure supplement 3. One-way ANOVA was performed with a Dunnett's posttest using GraphPad Prism9. For normalized intensity, all individual mutant cell line values were normalized to their paired control values. Average percent responders are presented. Bars represent the mean +/- SEM. One-way ANOVA with paired comparisons was performed with a Sidak's posttest for specific comparisons of normalized values using GraphPad Prism9. All generated cells lines were considered for the multiple comparisons.
(**C**) Phosphorylation intensity of pCD3ζ for T1 and T1$^{\Delta bind}$ (left), normalized pCD3ζ intensity for T1 and T1$^{\Delta bind}$ (center), and % responders of pCD3ζ for T1 and T1$^{\Delta bind}$ (right) were performed and analyzed as in B, with the exception that the open symbols represent data from a single experiment whereas the closed symbols represent

aggregate data from three independent experiments. Two-tailed t tests were performed to compare the single T1 vs $T1^{\Delta bind}$ samples as no other samples were collected in parallel.

Figure 3. The GGXXG and CV+C motifs are key determinants of CD4 function.
(**A, B**) Representative IL-2 production is shown in response to a titration of MCC peptide from one experiment (left). Experiments were performed in triplicate and each symbol equals the mean +/- SEM at that peptide concentration. AUC analysis for the dose response is shown as a measure of the response magnitude for the average of three independent experiments performed with one independently generated set of cell lines (center). The average response to a low dose (41nM) of peptide is shown as a measure of sensitivity for three independent experiments performed with one independently generated set of cell lines (right). Results are representative of those obtained with at least three independently generated sets of cell lines. One-way ANOVA was performed with a Dunnett's posttest for comparisons with WT and T1 samples, and a Sidak's posttest for comparisons between selected samples.

Figure 4. The GGXXG and CV+C motifs reduce pCD3ζ levels.
(**A**) Phosphorylation intensity of CD3ζ for T1 and T1-TMD (left), T1 and T1-Palm (2C) (center), and T1 and T1-TP (2C) (right) are shown for independently generated pairs of (connecting line) T1 and T1-TMD (left), T1 and T1-Palm (2C) (center), and T1 and T1-TP (2C) (right) cell lines. Each pair of lines (connected closed symbols) was tested in three independent experiments (technical replicates). The data from those experiments was aggregated, and the symbols represent the mean intensity of the aggregated pCD3ζ intensity values. One-way ANOVA was performed with a Dunnett's posttest using GraphPad Prims 9.
(**B**) Data for each cell line in **A** are shown as the average pCD3ζ intensity for all T1-TMD (left), T1-Palm (2C) (center), and T1-TP (2C) (right) cell lines normalized to their paired T1 control. Dotted line is the normalized pCD3ζ intensity for $T1^{\Delta bind}$ as a visual reference point for the contributions of CD4-pMHCII interactions. Bars represent the mean +/- SEM. One-way ANOVA was performed with a Sidak's posttest for specific comparisons using GraphPad Prims 9.
(**C**) The average % responders for phosphorylation of CD3ζ is shown for T1-TMD (left), T1-Palm (2C) (center), and T1-TP (2C) (right) compared to the average of their paired T1 control lines.
Bars represent the mean +/- SEM. One-way ANOVA was performed with a Sidak's posttest for specific comparisons using GraphPad Prims 9.

Figure 5. The (C/F)CVRC motifs reduces proximal TCR-CD3 signaling.
(**A**) Phosphorylation intensity of CD3ζ for T1 and T1-Palm (3C) (left) and T1 and T1-TP (3C) (right) are shown for independently generated pairs of (connecting lines) T1 and T1-Palm (3C) (left) and T1 and T1-TP (3C) (right) cell lines. Analysis was performed as in Figure 4A.
(**B**) Data for each mutant cell line in **A** are shown as the average pCD3ζ intensity values for T1-Palm (3C) (left) and T1-TP (3C) (right) normalized to their paired T1 controls. The dotted line represents the normalized phosphorylation CD3ζ intensity for $T1^{\Delta bind}$ as a

1122 visual reference for the contributions of CD4-pMHCII interactions. Analysis was
1123 performed as in Figure 4C.
1124 (**C**) Average % responders for phosphorylation of CD3ζ is shown for T1-Palm (3C) (left)
1125 and T1-TP (3C) (right) are shown compared to the average of their paired T1 control.
1126 Analysis was performed as in Figure 4C.
1127
1128

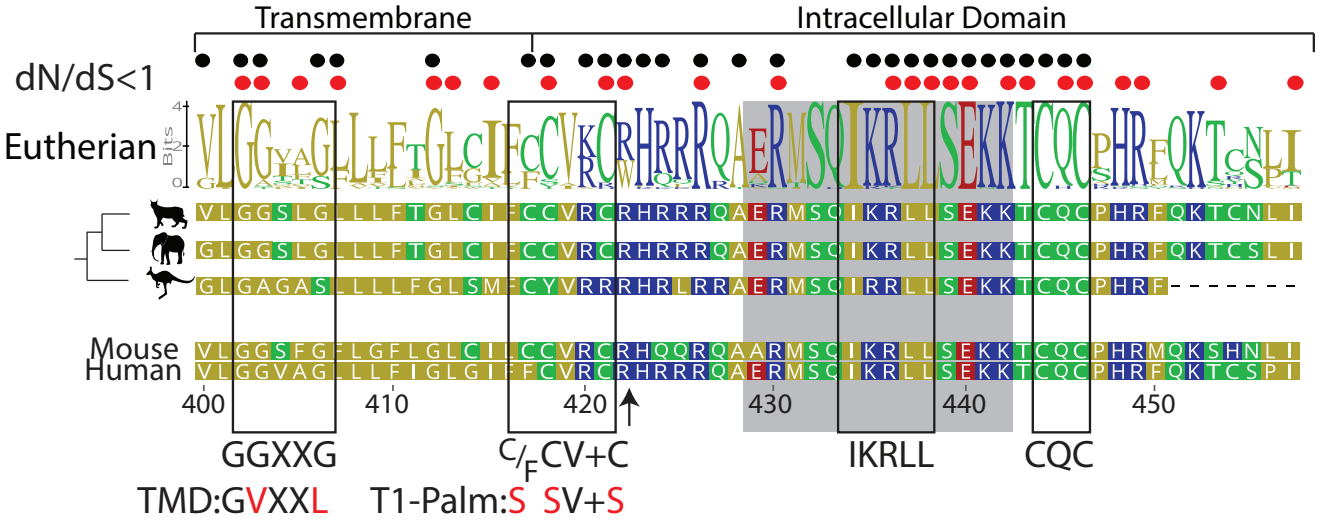
Transmembrane
Intracellular Domain
dN/dS<1
Eutherian
Bits
Mouse
Human
400
410
420
430
440
450
GGXXG
C/F CV+C
IKRLL
CQC
TMD:GVXXL
T1-Palm:S SV+S

Figure 1

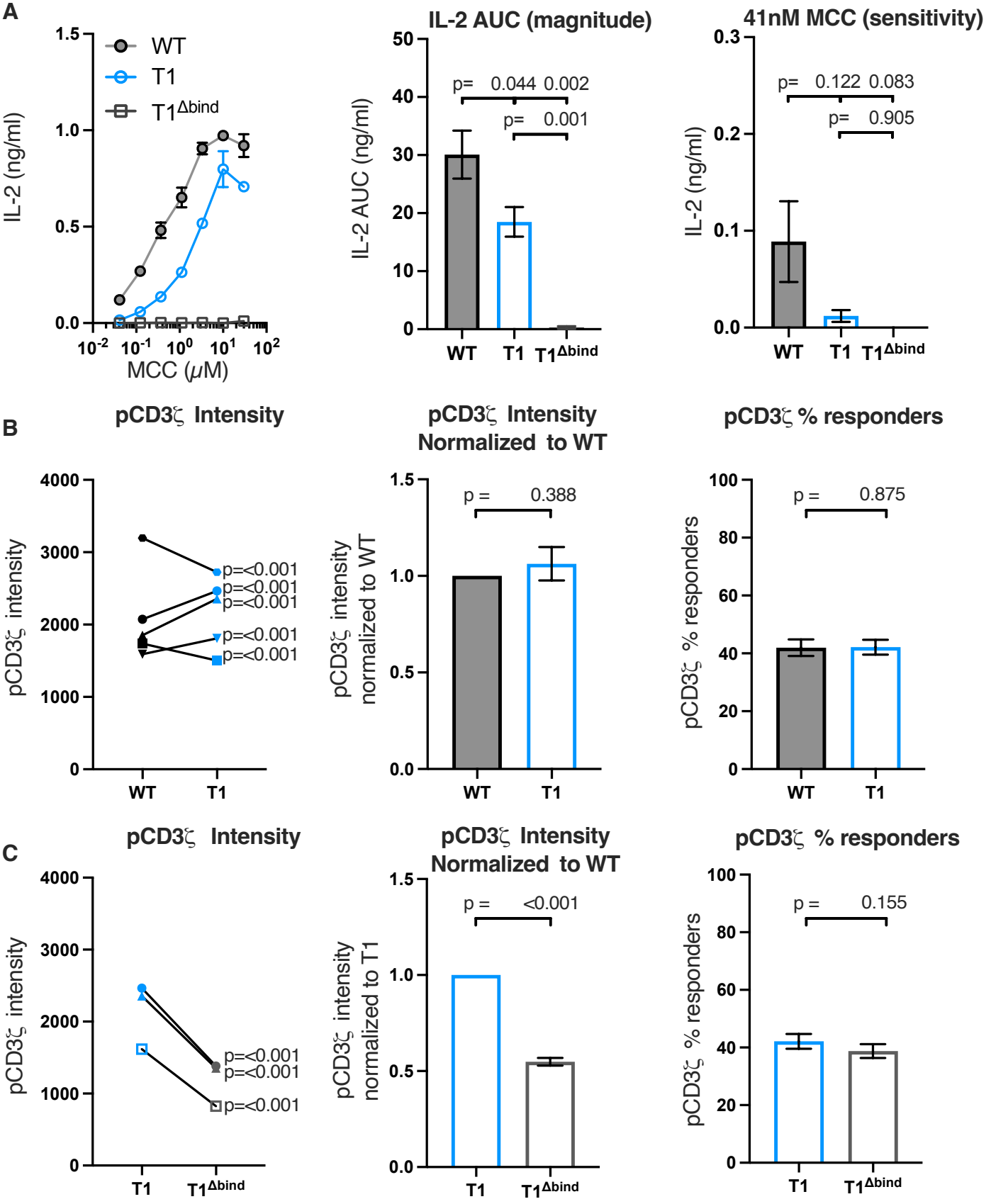
A
WT
T1
T1Δbind
IL-2 (ng/ml)
MCC (μM)
IL-2 AUC (magnitude)
IL-2 AUC (ng/ml)
p= 0.044 0.002
p= 0.001
41nM MCC (sensitivity)
p= 0.122 0.083
p= 0.905
B
pCD3ζ Intensity
pCD3ζ intensity
p=<0.001
pCD3ζ Intensity Normalized to WT
pCD3ζ intensity normalized to WT
p = 0.388
pCD3ζ % responders
p = 0.875
C
pCD3ζ intensity normalized to T1
p = <0.001
p = 0.155

Figure 2

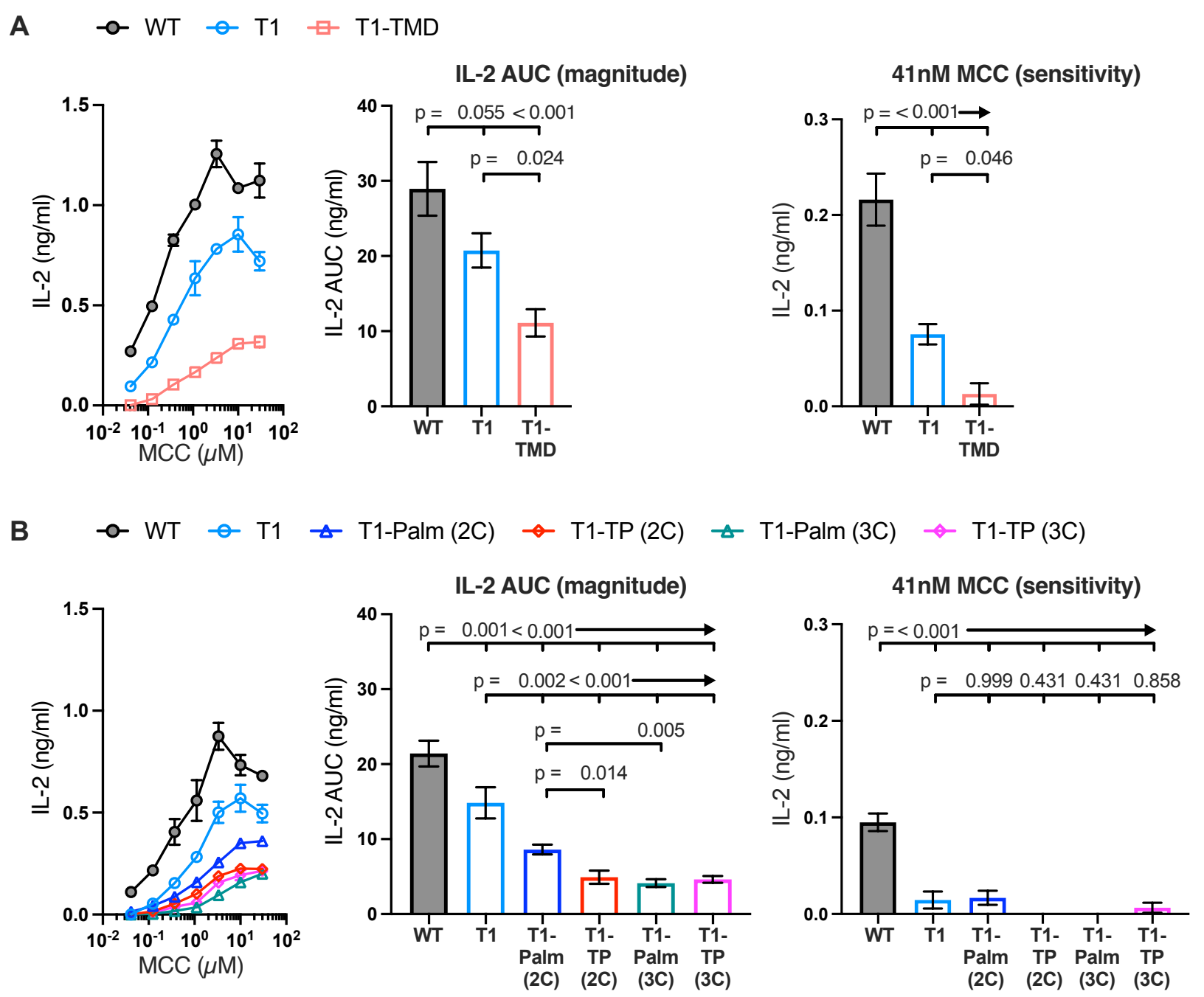
A
WT
T1
T1-TMD
IL-2 (ng/ml)
MCC (μM)
IL-2 AUC (magnitude)
IL-2 AUC (ng/ml)
p = 0.055
< 0.001
p = 0.024
WT
T1
T1-TMD
41nM MCC (sensitivity)
p = < 0.001
p = 0.046
B
WT
T1
T1-Palm (2C)
T1-TP (2C)
T1-Palm (3C)
T1-TP (3C)
p = 0.001
< 0.001
p = 0.002
< 0.001
p = 0.005
p = 0.014
p = < 0.001
p = 0.999 0.431 0.431 0.858

Figure 3

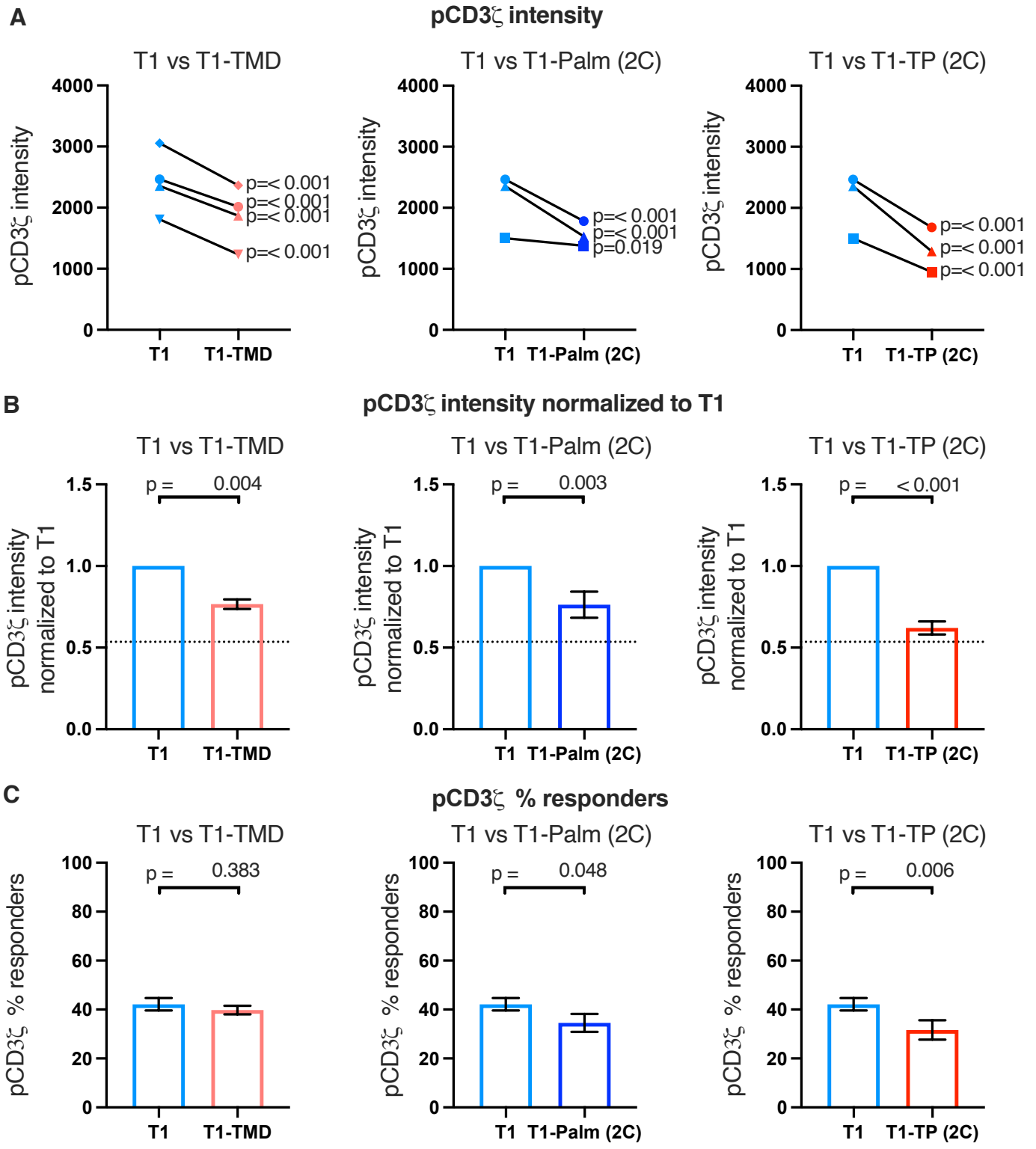
A
pCD3ζ intensity
T1 vs T1-TMD
T1 vs T1-Palm (2C)
T1 vs T1-TP (2C)
pCD3ζ intensity
4000
3000
2000
1000
0
p=< 0.001
p=< 0.001
p=< 0.001
p=< 0.001
p=< 0.001
p=< 0.001
p=0.019
p=< 0.001
p=< 0.001
p=< 0.001
T1
T1-TMD
T1-Palm (2C)
T1-TP (2C)
B
pCD3ζ intensity normalized to T1
pCD3ζ intensity normalized to T1
1.5
1.0
0.5
0.0
p = 0.004
p = 0.003
p = < 0.001
C
pCD3ζ % responders
pCD3ζ % responders
100
80
60
40
20
0
p = 0.383
p = 0.048
p = 0.006

Figure 4

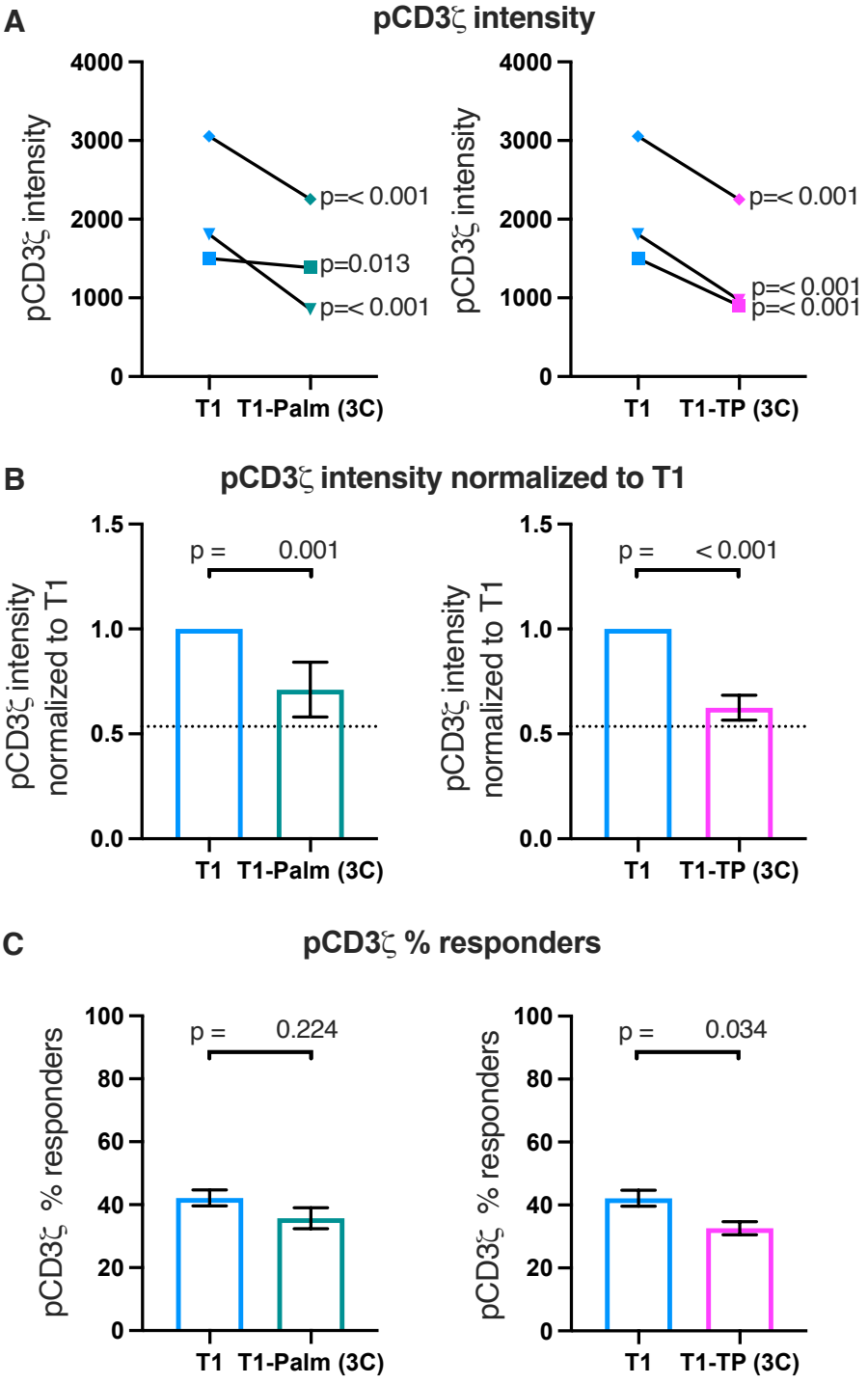
A
pCD3ζ intensity
pCD3ζ intensity
4000
3000
2000
1000
0
p=< 0.001
p=0.013
p=< 0.001
T1
T1-Palm (3C)
p=< 0.001
p=< 0.001
p=< 0.001
T1
T1-TP (3C)
B
pCD3ζ intensity normalized to T1
pCD3ζ intensity normalized to T1
1.5
1.0
0.5
0.0
p = 0.001
T1
T1-Palm (3C)
p = < 0.001
T1
T1-TP (3C)
C
pCD3ζ % responders
pCD3ζ % responders
100
80
60
40
20
0
p = 0.224
T1
T1-Palm (3C)
p = 0.034
T1
T1-TP (3C)

Figure 5

Table 1. Motifs and mutants analyzed in this study.

Motif location/known function	Mutant Names	Mutated Motif	Residue Mutations
C-terminally truncated CD4	T1	Ends at R422	R422 is the last residue
Extracellular D1 C"-strand (binds pMHCII)	$T1^{\Delta bind}$	GKGVLIR	K68D, V70D, L71S, I72D, R73S
TMD/Protein or cholesterol interactions	T1-TMD	GGxxG	G403V, G406L
Juxtamembrane/Palmitoylation	T1-Palm (2C)	CV+C	C418S, C421S
Juxtamembrane/Palmitoylation	T1-Palm (3C)	CCV+C	C471S,C418S, C421S
TMD+Palm/raft localization	T1-TP (2C)	GGxxG, CV+C	G403V, G406L, C418S, C421S
TMD+Palm/raft localization	T1-TP (3C)	GGxxG, CCV+C	G403V, G406L, C417S, C418S, C421S

Table 2. All values presented as percent of WT control (truncation average/WT average x 100) for normalized values.

Mutant Names	IL-2 magnitude	IL-2 sensitivity	Normalized pCD3ζ intensity	Normalized % Responders pCD3ζ	Normalized pZap70 intensity	Normalized % Responders pZap70	Normalized pPlcγ1 intensity	Normalized % Responders pPlcγ1	Lck DRM AUC	Lck Total AUC	Lck DSM AUC	CD4 expression	CD4 endocytosis
WT	100	100	100	100	100	100	100	100	100	100	100	100	100
T1	61.46	13.52	106.30	95.20	106.10	102.20	104.40	112.60	28.81	19.22	16.08	110.09	14.30

Table 3. All values presented as percent of T1 control (mutant average/T1 average x 100) for normalized values.

Mutant Names	IL-2 magnitude	IL-2 sensitivity	Normalized pCD3ζ intensity	Normalized % Responders pCD3ζ	Normalized pZap70 intensity	Normalized % Responders pZap70	Normalized pPlcγ1 intensity	Normalized % Responders pPlcγ1	Lck DRM AUC	Lck Total AUC	Lck DSM AUC	CD4 expression	CD4 endocytosis
T1	100	100	100	100	100	100	100	100	100	100	100	100	100
T1$^{\Delta bind}$	1.53	0.00	54.86	91.39	71.96	111.9	74.32	106.8	ND	ND	ND	73.93	38.71
TMD	53.54	17.05	76.68	94.23	88.36	98.77	88.24	107.40	62.36	92.97	110.94	131.10	3.63
Palm (2C)	57.99	116.07	76.35	94.09	86.17	93.03	92.09	98.09	274.03	139.40	130.91	80.30	-98.00
TP (2C)	33.11	0.19	62.06	85.61	79.79	75.58	82.57	83.34	121.39	113.03	114.98	96.54	47.50
Palm (3C)	27.84	0.19	71.09	94.76	86.32	76.82	80.37	88.62	137.57	94.34	92.07	87.58	6.99
TP (3C)	31.19	45.53	62.49	84.60	80.16	66.92	70.91	82.81	86.84	101.20	102.74	79.59	-54.69